

DTIC FILE COPY

4

August 1990

LMSC-F40416

**MAGNETIC RESONANCE IMAGING
STUDIES OF PROCESS RHEOLOGY**

FINAL REPORT

SUBMITTED TO:

Strategic Defense Initiative Organization
Innovative Science and Technology Office

Office of Naval Research
800 North Quincy Street
Arlington, VA 22217-5000

Atten: Dr. Richard S. Miller

AD-A225 814

DTIC
FILE
AUG 1990
D

PREPARED BY:

Materials Sciences Laboratory
Research and Development Division
LOCKHEED MISSILES & SPACE COMPANY, INC.
Palo Alto, California 94304

DISSEMINATION STATEMENT
Approved for public release
Distribution Unlimited

90 08 28 014

August 1990

LMSC-F40416

**MAGNETIC RESONANCE IMAGING
STUDIES OF PROCESS RHEOLOGY**

FINAL REPORT

SUBMITTED TO:

Strategic Defense Initiative Organization
Innovative Science and Technology Office

Office of Naval Research
800 North Quincy Street
Arlington, VA 22217-5000

Atten: Dr. Richard S. Miller

PREPARED BY:

Materials Sciences Laboratory
Research and Development Division
LOCKHEED MISSILES & SPACE COMPANY, INC.
Palo Alto, California 94304

MAGNETIC RESONANCE IMAGING STUDIES OF PROCESS RHEOLOGY

Research supported by the SDIO Innovative Science and Technology Office
and managed by the Office of Naval Research

G.A. Lo
S.W. Sinton
A.W. Chow

Lockheed Missiles and Space Co., Inc.
Lockheed Palo Alto Research Laboratory
3521 Hanover Street, O/93-50, B/204
Palo Alto, CA 94304

A.B. Kunz
M.J. Seel
S.A. Marshall
B.H. Suits

Michigan Technological University
Department of Physics
Houghton, MI 49931

Final Report for Contract Number N00014-86-C-0724

Prepared for
STRATEGIC DEFENSE INITIATIVE ORGANIZATION
Innovative Science and Technology Office
Washington, DC 20301-7100

OFFICE OF NAVAL RESEARCH
800 North Quincy Street
Arlington, VA 22217-5000

Accession For	
NTIS GRA&I	<input checked="" type="checkbox"/>
DTIC TAB	<input type="checkbox"/>
Unannounced	<input type="checkbox"/>
Justification	
AD-A203312	
By	
Distribution/	
Availability Codes	
Dist	Avail and/or Special
A-1	



TABLE OF CONTENTS

<u>Section</u>	<u>Page</u>
LIST OF FIGURES	ii
LIST OF ABBREVIATIONS	iii
1. INTRODUCTION	1
1.1 BACKGROUND	1
1.2 OBJECTIVES	1
1.3 SUMMARY OF PROGRAM ACTIVITIES	2
1.3.1 Summary of Program Activities prior to 1989	2
1.3.2 Summary of Program Activities for 1989 - 1990	5
2. PROGRAM PROGRESS DURING 1989 - 1990	7
2.1 Nuclear Magnetic Resonance Studies	7
2.1.1 NMR Imaging of Stationary Samples: Studies of Mixing and Flow in a Twin-screw Extruder	7
2.1.2 NMR Flow Imaging Studies	7
2.2 Theoretical Modeling	15
3. REFERENCES	17
Attachments:	
A. "Nuclear Magnetic Resonance Imaging Studies of.....A-1 Mixing in a Twin-Screw Extruder"	
B. "Stokesian Dynamics Simulation of Polyether-coated.....A-5 Particles in a Shear Flow"	

LIST OF FIGURES

<u>Figure</u>		<u>Page</u>
Figure 1:	Proton NMR images of PBAN/AS mixes from SIT.....	18
Figure 2:	X-ray images of samples of Figure 1.....	19
Figure 3:	Photo of NMR flow system and MOYNO pump.....	20
Figure 4:	Time-of-flight NMR imaging concept.....	21
Figure 5:	Time-of-flight NMR pulse sequence.....	22
Figure 6:	YZ slices of 3D flow image of water in 10-mm tube.....	23
Figure 7:	XZ slices of 3D flow image of water in 10-mm tube.....	24
Figure 8:	XY slices of 3D flow image of water in 10-mm tube.....	25
Figure 9:	Z velocity profiles along central Y trace of water in 10-mm tube.....	26
Figure 10:	Central XZ and YZ slices of 3D flow image of UCON/20% PMMA suspension in 1-inch pipe.....	27
Figure 11:	XY slices of 3D flow image of UCON/20% PMMA suspension in 1-inch pipe.....	28
Figure 12:	Summation of XY slices of Figure 11.....	29
Figure 13:	Z velocity distribution for UCON/20% PMMA in 1-inch pipe...	30
Figure 14:	Static image of UCON/20% PMMA in 2-inch pipe.....	31
Figure 15:	XY summation image of UCON/40% PMMA in 2-inch pipe.....	32
Figure 16:	Z velocity profile for UCON/40% PMMA suspension in 2-inch pipe.....	33
Figure 17:	XY summation image of UCON/40% suspension in 0.6-in pipe...	34
Figure 18:	Z velocity profiles along central X and Y traces for UCON/40% suspension in 0.6-inch pipe.....	35
Figure 19:	XY summation image of UCON/50% suspension in 0.6-in pipe...	36
Figure 20:	Z velocity distribution along central X trace of UCON/50% suspension.....	37
Figure 21:	Static XY image of UCON/50% PMMA suspension obtained immediately following cessation of flow.....	38

14-AUG-90

LIST OF ABBREVIATIONS

1-D	One-dimensional
2-D	Two-dimensional
3-D	Three-dimensional
AP	Ammonium Perchlorate
EM	Electromagnetic field
ESR	Electron Spin Resonance
LMSC	Lockheed Missiles and Space Co., Inc.
LPARL	Lockheed Palo Alto Research Laboratory
MR	Magnetic Resonance
MRI	Magnetic Resonance Imaging
MTU	Michigan Technological University
NG	Nitroglycerine
NMR	Nuclear Magnetic Resonance
NMRI	Nuclear Magnetic Resonance Imaging
ONR	Office of Naval Research
PBAN	Polybutadiene acrylonitrile
PEG	PolyEthylene Glycol
POM	PolyOxyMethylene
QM	Quantum Mechanics
RF	Radiofrequency
SD	Stokesian Dynamics
SIT	Stevens Institute of Technology

14-AUG-90

1. INTRODUCTION

This is the final report for the following contract, hereafter referred to as the Program. This research is sponsored by the Innovative Science and Technology Office of the Strategic Defense Initiative Organization, and managed by the Office of Naval Research (ONR). The Program is a joint effort between the Lockheed Palo Alto Research Laboratory (LPARL) and Michigan Technological University (MTU). Contract identification information is given below.

Contract Title: Magnetic Resonance Imaging Studies of Process Rheology
Contract Number: N00014-86-C-0724
Work Unit Number: Z400015SRS
Scientific Officer: Dr. R.S. Miller
Period of Contract: 9/30/86 to 8/15/90

Princ. Investigators: G.A. Lo (LPARL)
A.B. Kunz (MTU)

This report describes primarily activities and progress made on the program since issuance of the last Technical Report in 1988 [1]. Activities prior to that report are only mentioned below where necessary to explain the 1989 - 1990 activities. Detailed descriptions efforts in prior years can be found in the Program Technical Reports [1,2].

1.1 BACKGROUND

Improved processing methods are needed to achieve reliable, continuous production of high quality propellant. This has created a need for new technical approaches to on-line monitoring of propellant materials for quality assurance and process control. Current techniques are either invasive (direct probes), limited to dilute systems (X-ray or ultrasonics), or only capable of providing information on near-surface conditions (optical). The relatively new technology of magnetic resonance imaging (MRI) has the potential to non-invasively determine structural and compositional parameters and flow velocities throughout the volume of a material. MRI has not yet been exploited for propellant processing, in part because of limitations from existing techniques designed for applications to aqueous systems. This program, which is a joint program between Lockheed Palo Alto Research Laboratory (LPARL) and Michigan Technological University (MTU), has been established to make the necessary advances in MRI Technology. This program combines advanced MRI development with fundamental rheological investigations of particle-filled, polymer-based materials and with detailed numerical modeling studies of interactions at the molecular level. This program is designed to provide the basis for new tools for on-line propellant process monitoring, new predictive models for the flow behavior of highly filled polymer systems, and critical design guidelines for continuous processing procedures.

1.2 OBJECTIVES

The overall objectives of the Program were to develop experimental and

theoretical methods which will provide for improved methods of flow analysis as well as an improved understanding of the flow behavior of solid-particle-filled polymeric suspensions.

The objective of the experimental effort was to develop better magnetic resonance (MR) methods to detect and characterize inhomogeneities in uncured solid propellant. The specific experimental methods to be studied in the Program are nuclear magnetic resonance (NMR) and electron spin resonance (ESR). The goals were to develop magnetic resonance imaging methods with 100 μm or better spatial resolution for stationary propellant samples and to develop and characterize methods for imaging the flow of uncured propellants in process streams.

Besides assisting the MR experimental effort, the purpose of the rheological effort in this Program was to determine the effects of high solids loading on propellant flow behavior and their effects on continuous processing operations.

The objective of the theoretical modeling effort was to develop rigorous numerical models of macroscopic suspension flow in which the polymer-particle interaction physics are obtained from first principles with the aim of providing a more thorough understanding of the origin and nature of the observed macroscopic behavior of concentrated solid-particle-filled polymeric suspensions. The plan was to link together models from the atomistic level (Quantum Mechanics) and the particle level (Stokesian Dynamics) to yield an integrated predictive method based as much as possible on first principles.

1.3 SUMMARY OF PROGRAM ACTIVITIES

A brief summary of the Program's activities is given below. Significantly more detail is provided in references [1] and [2] and in Section 2 of this report, **PROGRAM PROGRESS**.

1.3.1 Summary of Program Activities prior to 1989

NMR Imaging at LPARL

LPARL received a high-power, multi-nuclear (including hydrogen) nuclear magnetic resonance (NMR) spectrometer in September 1987 and completed installation of the unit in January 1988. This instrument was used for both to image both stationary and flowing filled materials.

Imaging of stationary samples at LPARL involved primarily collaborations with Stevens Institute of Technology (SIT) in studies of suspension mixing and compounding in an extruder. Samples of a suspension of 60% ammonium sulfate (AS) in polybutadiene acrylonitrile (PBAN) were extracted from the SIT extruder and shipped to LPARL for NMRI analysis. The PBAN/AS suspension was designed to simulate the sort of materials and loading levels typically encountered in propellant processing. The basic idea of this effort was to determine the homogeneity of a suspension at different points in its processing history by imaging the polymer distribution, and then to use this information to quantitatively describe the mixing process for a particular mixer configuration. Lockheed contributed to this work by providing the imaging data and image analysis

14-AUG-90

techniques. This work is described in the previous Technical Reports and a number of publications [3,4] and was continued in 1989 - 1990.

The second major application of NMR to stationary samples was the detection of the solids distribution in solid-filled suspensions and cured materials. Since solids NMR imaging is a technology in its infancy, we were faced with the need to develop the methods required for our specific application. LPARL successfully demonstrated the basic concept of imaging aluminum particle concentration in an aluminum-powder-filled rubber with specialized "multi-pulse" NMR techniques. This technology was transferred to MTU for further development (see below) with the goal of producing multidimensional NMR images of the solids content in a propellant. Particle imaging is considered to be an important capability which it would be desirable to eventually develop. However, because particle imaging was considered to be of lower priority and requires more extensive development than flow imaging, a decision was made in 1989 to discontinue this part of the Program.

In the area of flow imaging efforts, LPARL set up a flow system designed to allow experiments on highly filled, viscous suspensions to be conducted. The heart of this system is a MOYNO progressive cavity pump capable of handling solid-filled suspensions and delivering appropriate pump rates in the viscosity range of interest. The capability that this system provides is unique in the field of NMR, giving LPARL a particular advantage in the study of suspension flow with NMR. The flow system is described in the 1988 Technical Report and summarized below. Preliminary experiments with the system and simple fluids were begun in 1988. In 1989 and 1990, a considerable amount of effort was expended on extending this technique to particle-filled suspensions, and our results are summarized below.

MRI at MTU

MTU completed construction of a high-field NMR spectrometer in February 1987 and designed and tested two NMR probes for imaging solid materials using the magnetic resonance of nuclei other than hydrogen. As reported in the 1988 Technical Report [1], MTU improved the design of their original gradient coils, resulting in a three-fold increase in resolution, and began work on implementing multi-pulse NMR methods in their laboratory. As mentioned above, this effort was discontinued in 1989.

A continuous-wave electron spin resonance (ESR) spectrometer at MTU was configured for imaging, and initial studies were carried out to determine the potential of the technique for propellant analysis. The continuous-wave electron spin resonance (ESR) imaging spectrometer at MTU was used to evaluate several candidate ESR label materials in a number of phantoms, and high-resolution images of suspensions were obtained for the first time by this technique. The spectrometer was then modified to a low-power pulse-echo configuration and initial studies of this setup were carried out. However, as for the solids NMR imaging case, it was decided that ESR imaging was of lower priority since the technique requires doping of the propellant to be imaged. Therefore, activity in this area was suspended in 1989.

14-AUG-90

Numerical Modeling Studies

There were two primary objectives of the modeling effort: (1) to develop and exercise a quantum mechanical (QM) model for atom clusters of relevant polymer binder and particle materials in order to provide interaction energies and relative forces of close polymer-polymer and polymer-particle units; and (2) to couple this model to a Stokesian Dynamics (SD) model in order to investigate how the quantum mechanically derived interaction potentials might effect macroscopic suspension rheological behavior. The resulting coupled model is an attempt to bridge the gap between our understanding of interactions at the molecular level with those that occur at particle and larger length scales.

Our preliminary studies (prior to 1988) were carried out using the QM and SD models in an uncoupled mode. The initial QM analyses of particle-filled polymeric suspensions yielded reasonable intramolecular polymer-polymer forces, and polymer-particle interaction forces. The attractive van der Waals potential between polymer units was determined, along with the chain slip barrier. The SD model was used to predict how various flow conditions would affect the evolution of structure in a suspension. The two models (QM and SD) were then linked together as described in reference [1] and summarized below. In the coupled model molecular-level interactions, as calculated from QM principles, are allowed to influence the evolution of the overall suspension system, as calculated by the SD model.

To couple the models, a linearized Lennard-Jones (L-J) particle-particle attractive force was added to the SD model. Derivation of the ratio of L-J to hydrodynamic forces [1,5] shows a dependence on the inverse of the particle radius. In polydisperse particle populations, therefore, the L-J force would be expected to exert a stronger influence on small (1-10 μm) particles than on large ones. Phenomena such as the tendency of particles to agglomerate or cluster could be affected by this force. This is of particular interest in propellant systems where fine particles often dominate the population. Since the L-J force becomes negligible when separation distances exceed about 50-100 \AA , only concentrated suspensions would be expected to show any significant effects of the L-J force.

A two-dimensional (2-D) Stokesian Dynamics (SD) code, named SDWL[©] (for Stokesian Dynamics with Walls), was acquired through Dr. J. F. Brady of the California Institute of Technology. This code was used to develop a prototype coupled Quantum Mechanical / Stokesian Dynamics (QM/SD) computer model, and this was completed in 1988. In order to model the intermediate (on the order of μm) and large (on the order of cm) scale effects of the material interactions, it was necessary to modify the SD model to include non-hydrodynamic interactions that are material-dependent. QM simulations performed in 1988 [5] on POM-POM, POM-AP and POM-AL interactions were used as basic input parameters needed to define the short-range forces in the coupled QM/SD. (POM = polyoxymethylene, AP = ammonium perchlorate, and AL = aluminum.) The physical premise of the model is that solid particles in a polymer suspension are coated with the polymer, and that the particle-particle interactions are influenced by the polymer-polymer interactions between particles. These interaction parameters defined the linearized L-J potential used to simulate short-

14-AUG-90

range forces in the SDWL calculations. Prior to this coupling effort, the SD model contained only hydrodynamic particle interactions that did not include parameters characterizing the chemical nature of the particles or the suspending fluid. This integration allowed us to study the effects of material-specific polymer and particle effects on the evolution of a particle suspension's microstructure. One output of the SDWL simulation of major interest is a prediction of the suspension's effective viscosity (η_e) as the microstructure evolves. Thus, it is possible to utilize the QM/SD tool to better understand the relationship between material specific microstructure and bulk material response.

Since the SD model simulations for multiple particle (>2) systems are built up from single particle-pair interactions, it was necessary to first test simulations of a single particle pair with and without the L-J force to confirm that the physics of their interaction is correct. This was done in 1988 and was reported in the last Technical Report [1]. As described in the next section, this initial work was extended to a 25 particle simulation in 1989.

1.3.2 Summary of Program Activities for 1989 - 1990

NMR Imaging of Stationary Samples: Studies of Mixing and Flow in a Twin-screw Extruder.

In 1989 and 1990 we continued our studies of suspension mixing in the SIT twin-screw extruder. New images of PBAN/AS suspensions were acquired and analyzed for suspension homogeneity. These samples were also examined by X-ray imaging to assess the concentration of voids, since it was discovered at SIT that bubbles can have a dominant effect on the rheology of this material. The results of this work are described in detail in Section 2.

A series of images were taken of samples supplied from SIT as part of a study of the flow patterns developed in a twin-screw extruder. In this study, carbon black powder was used to pigment sections of a thermoplastic which filled the extruder, and NMRI was used to determine how the carbon-black filled regions evolved as the extruder shaft was turned. This work was presented at the 1990 Society of Plastic Engineers Conference in Dallas, TX in 1990 and is published in the Conference proceedings [3]. A copy of that paper is attached to this report.

NMR Flow Imaging

The major accomplishment in the area of flow imaging during 1989 - 1990 was the successful imaging of flowing fluids and suspensions. The first flow images were collected in early 1989 on a pure fluid flowing in a pipe of 1 inch diameter and demonstrate the basic technique. These results (described in Section 2) were used to identify some of the capabilities and difficulties with flow imaging. Later work improved on the original technique and lead to useful density and velocity data for suspensions with up to 50% solids content. Results for these suspensions are also shown below. We attempt below to interpret the data, some of which exhibits unusual flow velocities and suspension composition, in terms of the bulk rheological behavior of highly filled suspensions undergoing inhomogeneous flow and in light of some recent theoretical

predictions of these systems. Our results also provide a demonstration of the expected resolving power and velocity detection range of the NMR technique.

Numerical Modeling Studies

The QM/SD model developed before was used to simulate the evolution of a 25 particle ensemble subjected to homogeneous shear forces. Two complete simulations were run over a long enough duration to elucidate differences in particle agglomeration and effective viscosity. In one simulation, van der Waals forces were excluded, i.e. this system involved hydrodynamic forces only. In the second, the linearized L-J potential was used to simulate the effects of van der Waals forces, and parameters for this force were derived from the earlier QM calculations on POM-POM and POM-particle interactions. The simulation which includes van der Waals forces shows significant particle agglomeration effects and the build-up of higher viscosity resulting from these effects when compared to the hydrodynamic-only case. These results have been published [6]; a copy of this paper is attached to this report. Some technical aspects of the modified SDWL program and its operation appear in Section 2. A copy of the program is available from MTU or LPARL on request.

2. PROGRAM PROGRESS DURING 1989 - 1990

This section covers progress made on the Program during the period from January 1, 1989 to May 31, 1990. Occasional reference is made to progress from previous years as required to clarify the discussion.

2.1 Nuclear Magnetic Resonance Studies

In this section we present results from the continued studies of mixing and flow in the SIT extruder and flow-imaging NMR data on pure fluids and suspensions acquired at LPARL.

2.1.1 NMR Imaging of Stationary Samples: Studies of Mixing and Flow in a Twin-screw Extruder

As discussed in the summary Section above, LPARL continued working with SIT on NMR imaging studies of mixing operations. The attached copy of reference [3] details some of the results and conclusions for the PBAN/AS. We also combined NMRI with X-ray imaging on two additional PBAN/AS samples to address the question of whether air voids existed in these materials to a significant extent. This was done because of some recent work done at SIT which suggested that air bubble entrainment during extruder processing could have important implications for suspension rheology. NMRI detects the polymer phase in PBAN/AS samples and reflects the homogeneity of the material by variations in intensity of the image. These variations can either arise because of non-uniform particle concentration (agglomerates, etc.) or voids since both represent an absence of PBAN. X-ray, on the other hand is more sensitive to voids since the smaller difference in X-ray absorption between clumps of pure AS and a mix of AS in PBAN will give less contrast than for a void surrounded by suspension.

Figure 1 shows two proton NMR images of two SIT PBAN/AS samples: one is well mixed while the other is not as is evident in these images. A sample of each mix was packed into a 10-mm NMR tube, and the images in Figure 1 are of .25 mm electronically selected slices taken perpendicular to the tube axis. Figure 2 show X-ray images of the same two samples. The plane of these images is parallel to the tube axis (and perpendicular to the NMR images in Figure 1), and, since there was no slice selection capability, these images are projections through the tube. Therefore the X-ray image intensity is a summation through the depth of the tube. Light areas are higher density and dark areas are lower density. As with the NMR images, the different mix quality is evident in these images. The many dark spots in the X-ray image of the poorly mixed suspension indicate the possibility of a high void content in agreement with the predictions from the rheological studies at SIT.

2.1.2 NMR Flow Imaging Studies

The purpose of the work performed was to define the capabilities and potential of NMR imaging as a technique for monitoring flow in highly filled suspensions of the propellant type. A secondary purpose was to use NMR flow imaging to study the effects of high solids loading levels on the flow behavior of propellant-like suspensions. Recent studies [7] have lead to the idea that the time-dependent rheological properties of

14-AUG-90

concentrated solid suspensions may be attributed to shear-induced particle migration in non-homogeneous flows (e. Consequently, a fundamental physical understanding of flow of suspensions demands an insight into the microstructure of the materials. Thus, our goal was to use NMRI to investigate the velocity and concentration profiles of suspensions in Poiseuille flows as a way of testing the proposed mechanisms.

To accomplish these goals, a series of experiments were performed in which either pure fluids or suspensions were flowed through straight pipes in a recirculating manner. In each experiment, the pipe passed through the NMR magnet and imaging probe. Two different imaging probes were used: the "microscope" probe, which gives high spatial resolution and has fast magnetic-field gradient switching capabilities but is limited to tube sizes below ~20 mm; and the "mini-imaging" probe which can handle much larger pipe sizes (~60 mm) but has limitations in gradient switching time and resolution. This equipment was used to investigate the range of velocities detectable and the sensitivity of NMR flow imaging. Since the tests were run on our current equipment, they represent the best results possible for this particular configuration. We indicate below some of the specific instrumental limitations we encountered and strategies for their amelioration.

Description of the Experiments

Flow system. For the smallest pipe size a simple impeller pump was used to drive water in a circulating loop through the micro-imaging probe. Figure 3 is a picture of the flow apparatus used for experiments on the larger pipe sizes and the mini-imaging probe. Because of the much higher viscosities of the oil-based fluids, a large, progressing-cavity (MOYNO) type pump was used. In this case, fluid was returned to the hopper of the pump so that a recirculating system was established, allowing long term acquisitions. The pump has a variable rate ring-cone drive mechanism and a motor tachometer to allow one to monitor the pump rate.

Materials. As mentioned above, three different fluids were imaged: water (containing a small amount of copper sulfate as a relaxation aid); a polyether oil (trade name = UCON) with 45% water; and suspensions of PMMA spheres in UCON + ~20% water. The PMMA spheres are polydisperse in size and have an average diameter of 130 μm . Sodium iodide was added to the suspensions in an appropriate amount to make the liquid density match that of the PMMA. Suspension loadings of 20, 40, and 50% were used.

Flow-imaging technique. A simple "time-of-flight" method was used to measure velocities in our experiments. This technique was originally developed by Kose, et al. [8] and has been further analyzed and modified by Majors, et al. [9]. The basic concept is depicted in Figure 4. At the start of the experiment, a "slice" of magnetization is prepared through the application of a radio-frequency (RF) pulse. This in essence "tags" the positions of those nuclei (in our case, the nuclei of hydrogen atoms) within the slice. As the material flows down stream (in this case, along the Z lab axis as defined in the Figure), the initial excited bolus deforms into a bullet shape because of the differences in velocities at various points within the slice. At some later time controlled by the experimenter, the slice is imaged. From a knowledge of

14-AUG-90

the flow time (duration of the experiment) and locations of each image picture element (pixel), the local velocity can be calculated. The image itself gives information on the density of nuclei within the slice. For a pure fluid, this should be uniform, while for a suspension, segregation of particles and fluid would cause a non-uniform image intensity.

The actual sequence of events used to form the image is depicted in Figure 5. This Figure shows the timing of RF and gradient pulses used to form either a 2 or 3 dimensional image of the slice. A detailed description of the technique appears in references [8] and [9], but there are a few important aspects which we must point out to make the discussion of the results clear. This sequence is designed to measure only one component of the velocities (along the Z direction). Other components could be measured with similar methods or others which have been devised for that purpose. With the velocities and flow rates of our experiments, the Reynolds numbers were usually low (less than 1800 for water, 5 for UCON oil/water, and unity for suspensions) and so laminar flow along the pipe direction was expected. Thus, we chose to concentrate on unidirectional velocity detection in our work to avoid the complication of full 3D velocity resolution.

The time of flight is defined as 4τ where τ is the delay between RF pulses as defined in Figure 5. For all the experiments described below, τ was set at 7.664 ms. The spatial resolution in the direction of flow is controlled by the Z gradient strength. Along with τ , this parameter determines the velocity resolution. Increasing either the Z gradient or τ would make slower velocities detectable. The upper range of velocity detection is ultimately set by the requirement that the nuclear magnetization must be fully polarized before the start of the experiment. This requires the nuclei to be moving slowly enough so that they can respond to the magnetic field as they enter the magnet. The magnetization equilibration rate is set by T_1 , the "spin-lattice" relaxation time constant. For our suspensions T_1 is typically 200 ms. The distance along Z over which the magnetic field ramps up from zero to its full value in our magnet is roughly 50 cm. Thus, even at the highest flow rates, there was ample time for polarization of incoming material.

In order to form a two or three dimensional image of the flowing slice of tagged nuclei, the sequence of Figure 5 must be repeated many times. Each repetition gives data for one row of pixels along Z. The entire sequence is repeated $n \times m$ times where n is the number of rows in each column parallel to X and m is likewise the number of rows in the Y direction. Thus, for a resolution of 64 x 64 pixels in each XY plane of a 3D image data set, the sequence must be repeated 4096 times. Each time the sequence is repeated, the X and Y gradients are varied to encode spatial information in these directions. Post processing of the data involves standard 2 or 3D Fourier transformation with application of appropriate noise-suppression filters. Each repetition of the sequence takes approximately 34 ms, but a delay of $3 * T_1$ (600 ms) between repetitions was required to allow spin-lattice relaxation to occur. Thus, a minimum of 41 minutes is required to collect a 3D image with X, Y, Z dimensions of 64 x 64 x 128 pixels. In some cases, we shortened the acquisition time by collecting only a 2D image wherein the intensity display is of the hydrogen density along either the X or Y directions projected into the corresponding perpendicular plane (YZ or XZ). For

some 3D images, the data matrix size was reduced to 32 x 32 x 128 for X, Y, and Z, respectively, trading off resolution for a reduction of acquisition time to 10.2 minutes. The excited slice thickness was 1 mm for experiments using the micro-imaging probe, and 3 mm for the mini-imaging probe.

Once a 3D image data set was collected and processed, velocities could be calculated by examining the image to determine the Z-axis displacement of the selectively excited slice at different X and Y locations. Dividing these displacements by the flight time (30.656 ms in our case) yields the local velocity for each portion of the slice. The entire image could be subjected to this calculation to arrive at a 3D mapping of the Z velocity field. Although this full calculation is in principle straightforward [9], we chose instead to do a much simpler calculation of the Z velocities along a slice parallel to either the XZ or YZ plane and through the center of the pipe (i.e. containing the central pipe axis). This velocity data is presented in the discussion below as plots of Z velocity vs. Y (or X) position along with the parabolic curves expected for laminar flow.

Results

The flow fields in four different pipe sizes were examined (i.d.'s = 0.4 in, 0.6 in, 1 in, and 2 in). The smallest pipe size was used to set up imaging parameters and test the techniques with the micro-imaging probe. This was a valuable exercise since it allowed us to test the imaging methods with more confidence in the early stages of our work. Once the basic methods were tested, flow images could be collected for the larger pipes with the mini-imaging probe.

The fluids imaged with the mini-imaging probe included a viscous mixture of a polyether oil and water and several suspensions made from an oil/water liquid base and solid poly(methyl methacrylate) (PMMA) spheres. The solids concentration in these suspensions ranged between 20 and 50%. The following table summarizes the NMR flow imaging experiments performed.

Table 1. NMR imaging experiments

Pipe Diam. (in/mm)	L/D (L=500 mm)	a/D (a=130 μ m)	water	UCON/ water	20% PMMA	40% PMMA	50% PMMA
0.4/10.2	49.2	0.0130	x				
0.6/15.2	32.8	0.0086				x	x
1.0/25.4	19.7	0.0051		x	x		
2.0/50.8	9.84	0.0026			x	x	

In Table 1, a is the average diameter of the PMMA spheres, D is the

14-AUG-90

diameter of the pipe, and L is the entrance length of the pipe to the imaging area. The ratios a/D and L/D are relevant parameters characterizing the flow conditions as is discussed below.

The results for the different combinations of fluid types and pipe sizes are given below. They clearly demonstrate that we are capable of detecting flow velocities in the range of 0.1 to 45 cm/s with the current set up. Additionally, the method simultaneously yields reasonably quantitative (with some restrictions particular to our equipment) density information. Detection of faster or slower velocities would be possible with minor modifications of the technique.

Water in 10-mm i.d. tube. Figures 6, 7, and 8 show the 3D image of a 1-mm thick slice of hydrogen magnetization in a stream of water flowing in a 10-mm id tube through the microscope probe. The 3D data matrix had dimensions of $32 \times 32 \times 128$ (X, Y, Z), and the entire image took 17 min. to acquire. Figure 6 shows the 32 slices parallel to the YZ plane. The curved shape of the slice is clearly evident in these images (flow is from right to left). Figure 7 is a similar display of the slices parallel to the XZ plane. Figure 8 shows selected slices parallel to the XY plane and a summation of these slices which represents a "projection" of the hydrogen density within the moving slice onto the XY plane. The uniformity of this image demonstrates that quantitative density information can be obtained from a flowing stream with the microscope probe.

Figure 9 is a plot of the Z velocities across the midplane slice parallel to the YZ plane calculated from the data of Figure 6 and from an image at a higher flow rate. The curves are parabolas fit to the data by varying only the maximum (centerline) velocity. The agreement is quite good, allowing for the limited resolution along Z in the NMR image.

UCON + 20% PMMA spheres in 1-inch pipe. A number of images were acquired of the UCON + 20% PMMA flowing at various rates in the 1 inch pipe configuration. Figures 10 and 11 show some selected slices taken through one such image at a fairly high flow rate. For this image the pixel dimensions were $64 \times 64 \times 128$ (X, Y, Z), and the total acquisition time was 41 min. Figure 10 shows expanded views of the central XZ and YZ slices. (The flow direction was the same as in the case of the water images above. However, the direction of the Z gradient in the mini-imaging probe is opposite to that in the microscope probe. Thus, the curvature of the slices in Figure 10 is opposite to that in Figures 6 and 7.) The excited slice thickness in this case was 3 mm. The resolution in the X and Y directions is .52 mm/pixel while in the Z direction it is .55 mm/pixel. Figure 11 shows selected slices parallel to the XY plane. Figure 12 is a summation of the intensity in these slices. As can be seen, the material appears to be uniform from the even distribution of image intensity. Note the dark spot in the lower left corner. We believe this was from a bubble or some other inclusion which did not move during the 41 min. acquisition time. Static images (see below) showed that the material is certainly not free of bubbles.

Figure 13 shows a plot of the calculated Z velocities along the central Y slice as for the earlier plot. Once again, the fit to a parabola is excellent with minor deviations most likely caused by limits in

14-AUG-90

resolution.

UCON + 20% PMMA spheres in 2-inch pipe. To test the capabilities of the LPARL instrument on large sized pipes, the UCON/20% PMMA suspension was also run in a 2-inch pipe. Figure 14 shows a static XY image (no flow) of the 20% suspension in a 2-inch pipe. Two things are immediately apparent from this image. First, as mentioned above, it is clear that this suspension contained bubbles. This was expected to some degree since this viscous suspension was not mixed under vacuum. This does not adversely effect the ability to detect the average (steady state) velocities by the time-of-flight technique, but does make apparent the fact that the density information obtained from a 3D flow image is an average of what passes through the imaging region during the acquisition period. Thus, only averaged density features are seen, and individual features, such as the bubble mentioned above, can only arise from something which, on the average, remains constant during acquisition. Much faster imaging techniques, some of which are beginning to appear in the literature, would be necessary to obtain an instantaneous "snapshot" of the material density.

The second thing that becomes apparent from Figure 14 is that the detection sensitivity of our mini-imaging probe is not uniform over the 2 inch diameter of the pipe. This fact is evident in the gradual variations in intensity moving from the center to the outer edge of the pipe and is caused by the imperfect nature of the RF field generated by the probe. This is essentially an instrument problem and undoubtedly other probe designs might perform better. Although problematic for absolute density measurements, this feature of our probe does not destroy its ability to image velocities in large-diameter flows as we show below. These RF inhomogeneity features do not appear in the 1 and .6 inch pipe images because the XY fields of view in those cases avoids the worst regions of inhomogeneity.

UCON + 40% PMMA in 2-inch pipe. Following the experiments on the 20% suspension, the PMMA concentration was increased to 40%. Figure 15 is a density image obtained by summing XY slices from a 3D data set as described above. Once again, intensity variations attributable to RF inhomogeneities are evident, but otherwise, the average density appears uniform. Figure 16 is a Z velocity profile through the tube center calculated from the image data. The velocity distribution is clearly parabolic despite the limited resolution along Z achieved for this flow rate.

UCON + 40% PMMA in 0.6-inch pipe.

Figure 17 is a display of the summed XY image intensity of a flowing stream of the 40% suspension in the smallest tube studied with the mini-imaging system. Despite the smaller number of pixels, resolution in the XY plane is actually almost a factor of 2 higher in this image compared with Figure 15 (0.61 mm/pixel vs. 1.1 mm/pixel). Across the image is a display of the pixel intensities in row # 19 which demonstrates the non-uniform nature of the intensities. This feature is not a result of RF inhomogeneity as in the case of a 2-inch pipe. Images of static suspensions in the 0.6-inch pipe do not show this sort smooth increase in intensity toward the pipe center. Thus, the result shown in Figure 17 is

14-AUG-90

somehow caused by flow. We give some possible explanations below.

Figure 18 shows plots of the central Z velocity distributions along the X and Y directions from the 3D image corresponding to Figure 17. In both plots two parabolas are shown to demonstrate by inspection that no one parabola uniquely fits all the velocity data. The velocity distribution in both directions appears to be "blunted" with slower than expected velocities toward the center of the tube. This sort of distribution has been predicted from current theories [10] of suspension rheology and is thought to arise from flow-induced particle migration. In these theories, particles are predicted to diffuse away from regions of high shear rate in an inhomogeneous flow. Thus, particles should migrate to the center of the tube and a plug-like flow should develop. Although we detected what appears to be the onset of plug flow in the velocity profile, the implied density distribution of Figure 17 does not agree with a concentration of particles toward the tube center. (Recall that the images are of the polymer and not the beads.) We return to this point in the Discussion Section below.

UCON + 50% PMMA in 0.6-inch pipe.

Figure 19 is a display of the summed XY image intensity of a 50% PMMA/UCON suspension in the 0.6-inch tube. As with the 40% suspension, we once again see a smooth gradation of intensity increasing from the edge to center of the tube. Figure 20 is the velocity profile along one direction, and again it appears "blunted."

Figure 21 is an XY image of the 50% suspension immediately following the cessation of flow. Once again, the image shows a non-uniform intensity distribution, although it is quite different from that in Figure 19 and the overall variations are much smaller. (The crescent shaped features in this image outside the tube are from signals "folded over" from a larger tube concentric with the 0.6-inch tube which was used to center and provide support for the smaller tube. These features do not interfere with either the static or flow image of the small tube.) The discrepancy between the intensity images during and following flow might have a number of possible explanations. It is unlikely that any steady-state concentration variations would dissipate quickly in a fluid of such high viscosity as containing relatively large particles. Therefore, we cannot ascribe the image differences to a remixing of the suspension through rapid diffusion of particles. Another possible explanation arises when one recalls that the intensity display of Figure 19 is an average of what flows through the pipe during the entire data acquisition and so might reflect periodic or random fluctuations in material properties. This and other potential explanations for our observations are addressed below.

Discussion

Our results serve to delineate some of the basic capabilities of NMR flow imaging as applied to the study of flow of suspensions. For the most part, the density and velocity profiles obtained agree with what is expected for simple Poiseuille flow. The velocity profile of a suspension in Poiseuille flow is determined not only by the particle concentration (c) but also by the values of a/D and L/D (where a is the

particle average diameter, L and D are the entrance length and diameter of the pipe). At low values of c and a/D , the velocity is parabolic. Deviation from the parabolic distribution, with slower velocities at the center of the pipe, is observed as c , a/D , and/or L/D values are increased. For instance, the 40% suspension exhibits a blunted profile for high values of a/D and L/D (0.0086 and 32.8, respectively) with the 0.6-inch pipe but not for the lower values ($a/D=0.0026$ and $L/D=9.84$) in the case of the 2-inch pipe. Our velocity profile measurements using NMRI are in good agreement with those reported by Karnis, et. al. [11] using direct visualization of tracer particles in flow.

The blunting of the velocity profile of concentrated suspensions in Poiseuille flow is consistent with predictions calculated by Leighton [10] based on the shear-induced particle migration mechanisms proposed by Leighton and Acrivos [7]. The dependence on a/D and L/D values is presumably either a result of wall effects or a manifestation of the "induction length" needed for particle concentration across the pipe to reach steady state (such that particle migration due to the shear rate gradient is balanced by that due to the concentration gradient). This induction length is not the same as the "transition length" needed for the boundary layer to reach the center of the pipe in laminar flow such that a fully developed flow profile is established. For a Newtonian fluid, the normalized transition length, x_t/D , can be approximated by $(Re/20)$. In our experiments on suspensions, the normalized entrance length (L/D) in all cases is much larger than the calculated x_t/D (see Table 1).

Our flow imaging results also indicate that the blunted velocity profile is accompanied by a non-uniform NMR intensity profile across the pipe. However, the intensity profile obtained during flow (with higher intensity in the center) is different than that obtained immediately after the cessation of flow. Due to the high viscosity of the suspending fluid and the large particle size, diffusion of particles should be very slow and for all practical purposes, the microstructure of the suspension induced by flow should be preserved after flow cessation.

So far, we have assumed that the flow NMR image intensity corresponds directly to the density (or equivalently, the concentration) of the liquid portion of the suspensions. If this is true, then the local particle concentration can be taken as the inverse of the gray scale of our images. This would imply that for the 40 and 50% suspensions in the smallest tube particles are concentrated toward the outside during flow. This is the opposite the expected concentration profile based on theory. This conflict with theory, and the apparent discrepancy between the flow and static image intensity distributions mentioned above, require us to take a closer look at the meaning of flow image intensity.

One possible interpretation of our results is that the intensity profiles we see do in fact reflect the true liquid density and that there is some aspect to the flow behavior which we have not yet considered such as some periodic or random fluctuation which yields the averaged observed profiles. This would seem unlikely for the simple Poiseuille flows of our system. Another possibility is that image intensity does not actually correspond directly to proton density. There are two possible ways in which this might come about. First, the flow image sequence may

14-AUG-90

not be functioning properly. The sequence (Figure 5) is designed to yield an image where the effects of motion in the presence of a field gradient have been compensated so that the signal that is detected can be correctly mapped into spatially resolved density. This requires critical adjustments of the sequence timing parameters and gradient pulse shapes. Any errors in these adjustments could lead to distortions in the image shape and intensity and these distortions would show up stronger at higher velocities. We do not believe misadjustments of the sequence account for our intensity observations for the following reason. The image of the 20% suspension in the 1-inch pipe was collected with the same adjustments as the 0.6-inch pipe and at comparable maximum velocity (Figure 13) and yet yields a uniform XY "density" image (Figure 12). Other data not shown here also support this argument. Thus, we believe the unexpected intensity distributions found for the highly loaded suspensions are not the result of errors in the imaging technique.

A second possible explanation is that the NMR signal does not actually reflect proton density but rather some other NMR parameter. It is well known that NMR image intensity can sometimes depend on the spin-spin (T_2) and spin-lattice (T_1) relaxation parameters. If these parameters vary within a sample, then they can potentially weight the image intensity away from a pure density measure unless precautions are taken to ensure that the image sequence takes much less time to execute than either T_1 or T_2 . It is also known that in suspensions T_1 and T_2 depend on the surface-to-volume ratio due to surface-induced magnetic relaxation [12,13]. Thus, if the local surface-to-volume ratio varies significantly as a result of gradients in the bead concentration and/or the bead size distribution across the pipe, magnetic relaxation effects could affect pixel intensity. This might account for our observations and explain the different images for flow and static conditions since these images were obtained with different sequences which used different durations and would therefore be subject to differences in T_2 weighting. Another possible source of relaxation weighting would be a velocity dependence on T_1 or T_2 although we know of no mechanism for such a dependence.

The issue of possible relaxation weighting could be addressed through a series of experiments to measure the relaxation times for suspensions with different bead content. If a significant dependence is found, this data could be used to calibrate NMR images as a way to recover pure density data. Additionally, forming T_1 or T_2 images may provide a useful means to measure local surface-to-volume variations in inhomogeneous suspensions. Such experiments are planned for the follow-on contract to this program.

2.2 Theoretical Modeling

The results for the 25 particle QM/SD simulation are summarized in Section 1 above and detailed in the attached copy of the joint MTU/LFARL publication. A description of the modifications implemented in the original SDWL code follows.

The molecular forces appropriate for polymer-coated particles are added to the original SDWL code as external forces. These forces are calculated and added to the hydrodynamic forces in a new subroutine, EXROC, according to equations (13) and (2) in reference [6], if the

14-AUG-90

variable IVDW is set equal to one (otherwise, the original SDWL code is executed). The new constants which define the van der Waals - like polymer - polymer interactions are (see equation (15) in reference [6]) are:

FNORMCC	Normalization factor for polymer-polymer interaction (e.g. 10^8).
XIOCC	Equilibrium distance between two polymer units (dimensionless), e.g. 6×10^{-4} , corresponds to four Angstroms for particles of radius 0.5 microns.
XIOCB	Equilibrium distance between polymer and particle
FNORMBC	Normalization factor for polymer-particle interactions.
CUTOF1	Upper limit of linear van der Waals interaction forces. Below CUTOF1 force is linear, above CUTOF1 is the XI^{*-5} region for sphere - sphere van der Waals interactions.
FCONA	Approximate depth of attractive force well in linear van der Waals region.
FCONR	Approximate height of repulsive force in linear van der Waals region.
COVER(I)	Coverage of polymer - polymer [covered - covered (CC)], or polymer - polymer [covered - bare (CB)] interaction for each particle. COVER(I) varies between 0.0 and 1.0.

Since the molecular forces change over a million-fold range for small surface separations, the time scale appropriate for hydrodynamic interactions does not capture the molecular force region. On the average, the time step has to be smaller by a factor of 1000 for molecular forces. Thus, there is an additional input parameter, DTLs, describing the ratio of large to small time steps (DTL/DTS).

In order to speed up the calculation, an automatic time step adapter has been built in. Depending on the maximum size of the molecular force as calculated in EXFORC, a flag is returned. This flag, IFLAG, sets the time step according to the following table.

IFLAG = 0	DT = DTL
IFLAG = 1	DT = DTS X 100
IFLAG = 2	DT = DTS X 10
IFLAG = 3	DT = DTS

This allows for a time step which is 10 times, 100 times, or 1000 times shorter than the "hydrodynamic" time step. The code was adapted to the SUN's FORTRAN 77 compiler by an automatic precompiler. A listing of the code is available from the MTU or LPARL upon request.

3. REFERENCES

1. "Magnetic Resonance Imaging Studies of Process Rheology," 1988 Technical Report for contract #N00014-86-C-0724. Doc. # LMSC-F277133.
2. "Magnetic Resonance Imaging Studies of Process Rheology," 1987 Technical Report for contract #N00014-86-C-0724.
3. S. W. Sinton, J. C. Crowley, G. A. Lo, D. M. Kalyon, and C. Jacob, "Nuclear Magnetic Resonance Imaging Studies of Mixing in a Twin-Screw Extruder," Paper presented at the 1990 Soc. Plastic Eng./ANTEC Conf., Dallas, Texas.
4. D. M. Kalyon, S. W. Sinton, C. Jacob, and R. Yazici, "The Effect of Air Entrainment on the Rheology of Concentrated Suspensions During Continuous Processing," to be submitted to J. Rheology.
5. M. Seel, D. T. Wadiak, and A. B. Kunz, Phys. Rev. B, 37, 8915 (1988).
6. M. Seel, D. T. Wadiak, A. B. Kunz, and S. E. Hill, "Stokesian Dynamics of Polyether-Coated Particles in a Shear Flow," Phys. Rev. A, in press.
7. D. Leighton and A. Acrivos, "Shear-induced migration of particles in concentrated suspensions", J. Fluid Mech., 181, 415 (1987).
8. K. Kose, K. Satoh, T. Inouye, and H. Yasuoka, "NMR Flow Imaging," J. Phys. Soc. Japan, 54, 81, 1985.
9. P. D. Majors, R. C. Givler, and E. Fukushima, "Velocity and Concentration Measurements in Multiphase Flows by NMR," J. Magn. Reson., in press.
10. D. Leighton, "Migration arising from gradients in shear stress: particle distributions in Poiseuille flow." NASA Conference Publication 3006, "Mixing and Demixing Processes in Multiphase Flows with Application to Propulsion Systems" held at AVNASA Marshall Space Flight Center, Alabama, February 25-26, 1988.
11. A. Karnis, H. L. Goldsmith, and S. G. Mason, "The kinetics of flowing dispersions: I. Concentrated suspensions of rigid particles," J. Coll. Interface Sci., 22, 531 (1966).
12. J. A. Glasel and K. H. Lee, "On the Interpretation of Water Nuclear Magnetic Resonance Relaxation Times in Heterogeneous Systems," J. Amer. Chem. Soc., 96, 970 (1974).
13. B. M. Fung and T. W. McGaughy, "Magnetic Relaxation in Heterogeneous Systems," J. Magn. Reson., 43, 316 (1981).

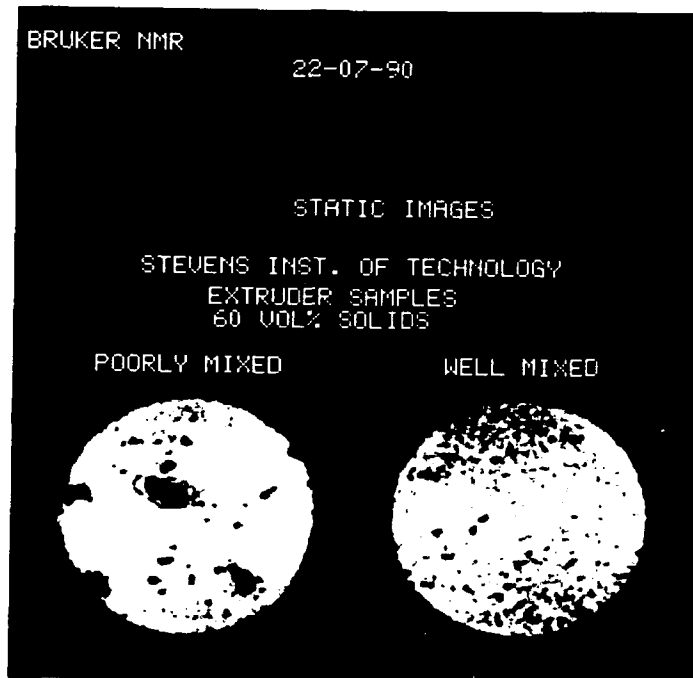


Figure 1: Proton NMR images of PBAN/AS mixes from SIT. These images are of 0.25 mm sliced cross sections of 10-mm tubes packed with each mix.



Figure 2: X-ray images of samples of Figure 1. The orientation is perpendicular to the slice direction of the NMR images and the intensities are a projection through the tubes.

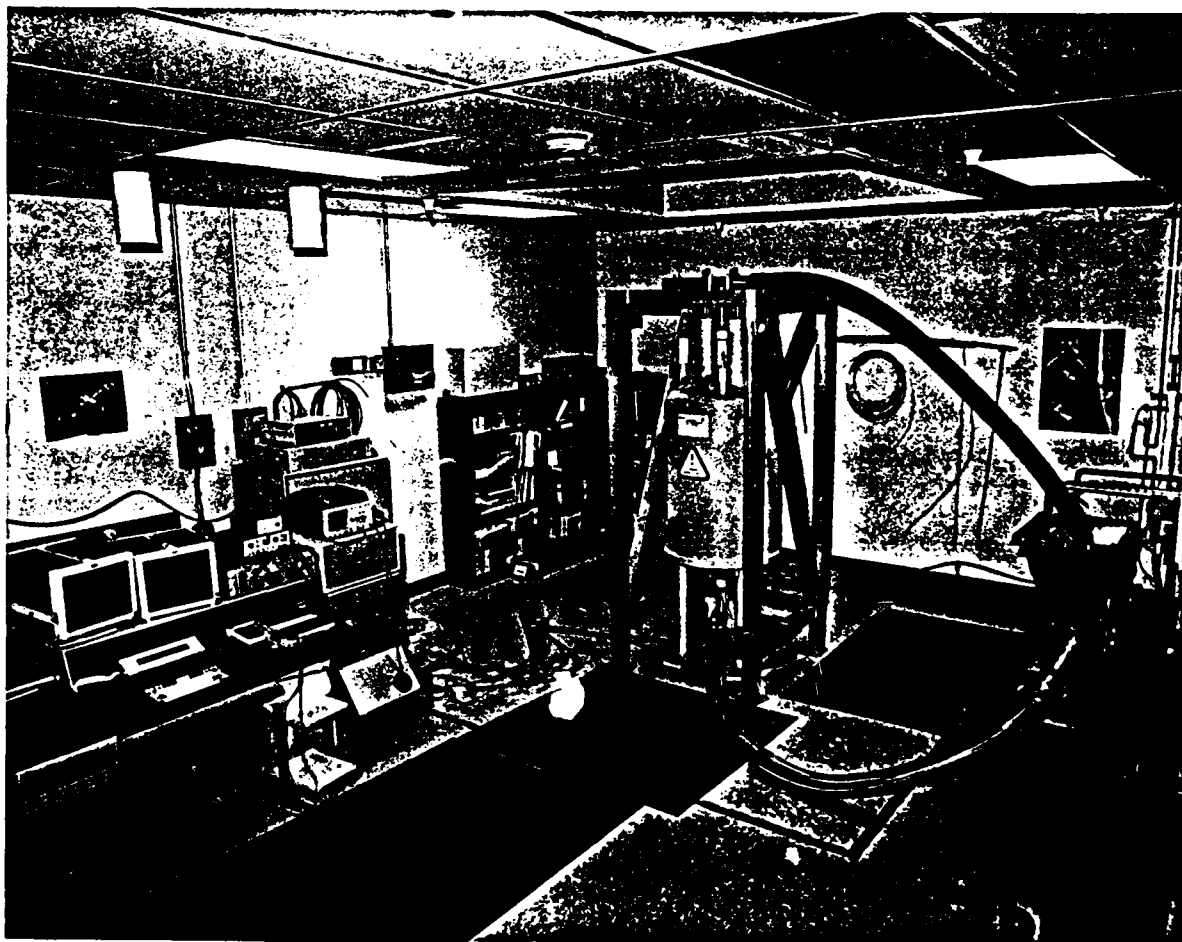
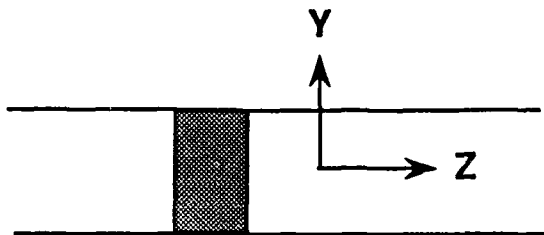
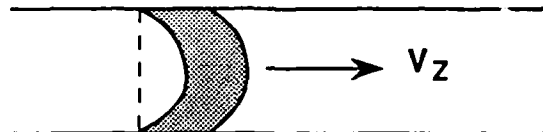


Figure 3: Photo of NMR flow system and MOYNO pump.



At time $t=0$, a "slice" of nuclear magnetization is excited.



After a period of time (the "flight" time) an image of slice, shaped by flow, is recorded.

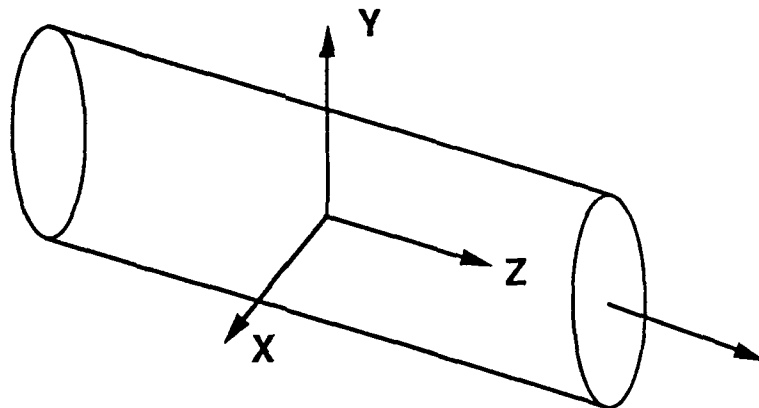
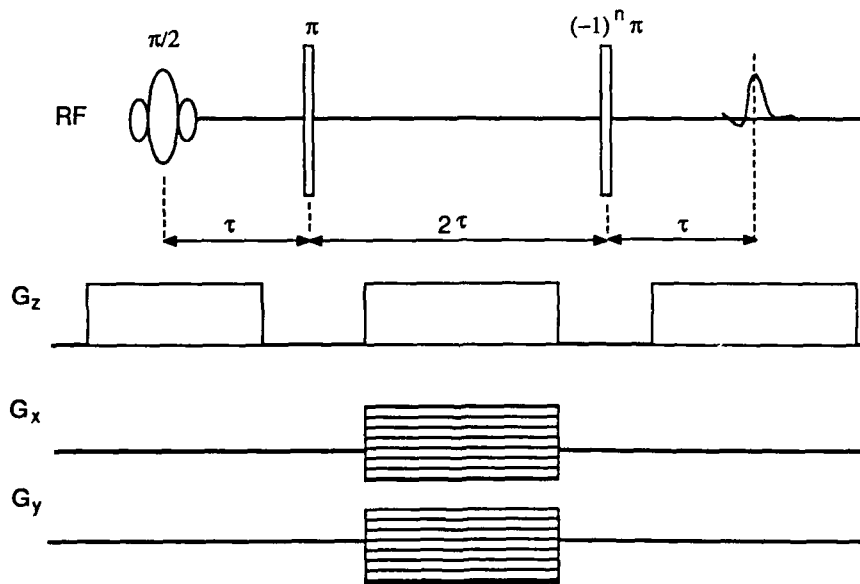


Figure 4: Time-of-flight NMR imaging concept. The coordinate system defines the axis of the images to follow.

SPIN-ECHO 3D FLOW COMPENSATED IMAGING



- Designed to compensate for constant velocities along Z direction
- Phase of second echo is independent of Z velocity
- Phase of second 180 pulse is alternated with phase-encode gradient steps to shift interference from stimulated echo to Nyquist edges of image.

Figure 5: Time-of-flight NMR pulse sequence.

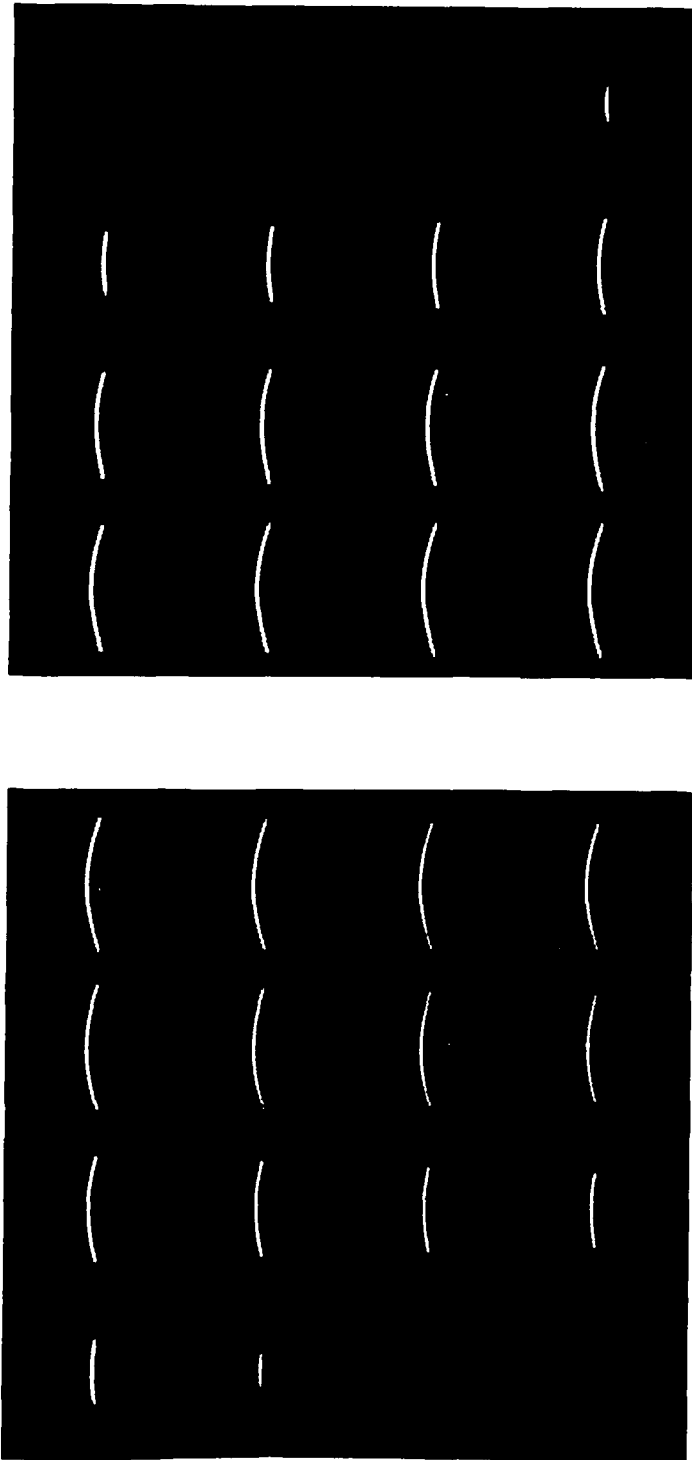


Figure 6: YZ slices of 3D flow image of water in 10-mm tube.

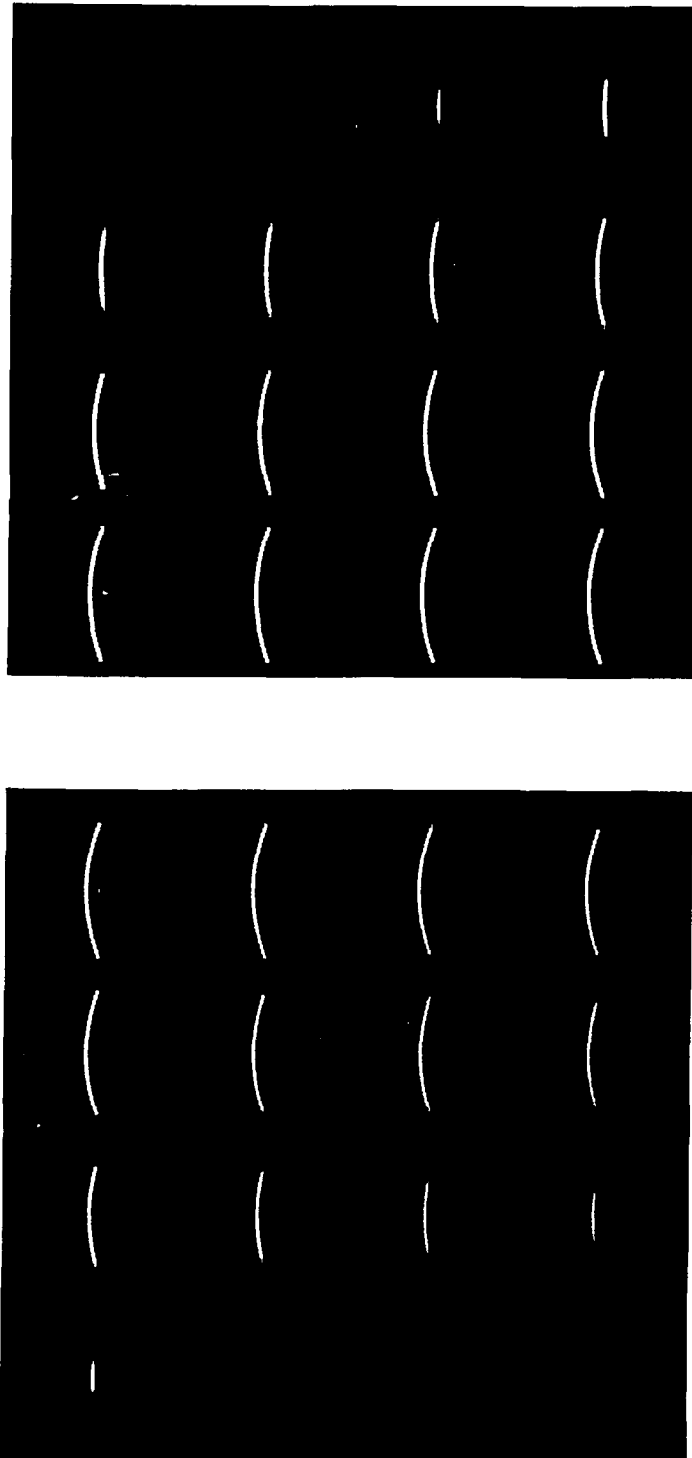


Figure 7: XZ slices of 3D flow image of water in 10-mm tube.

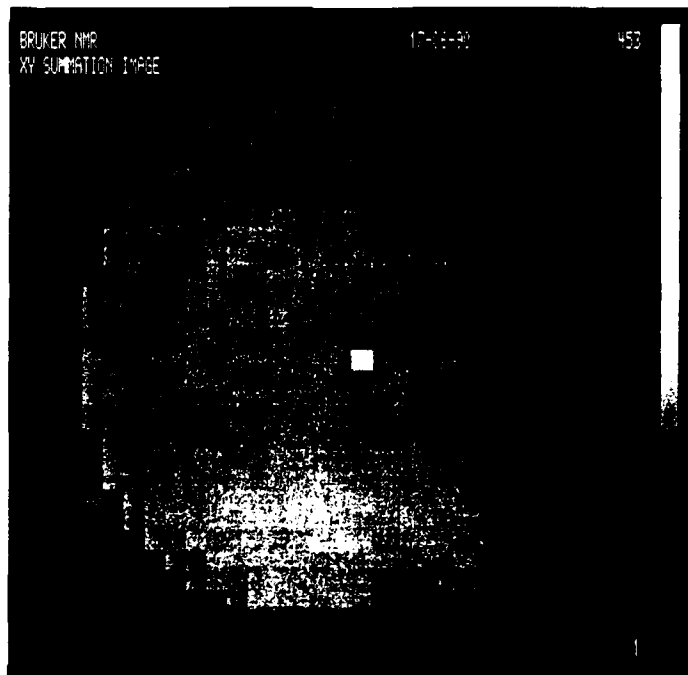
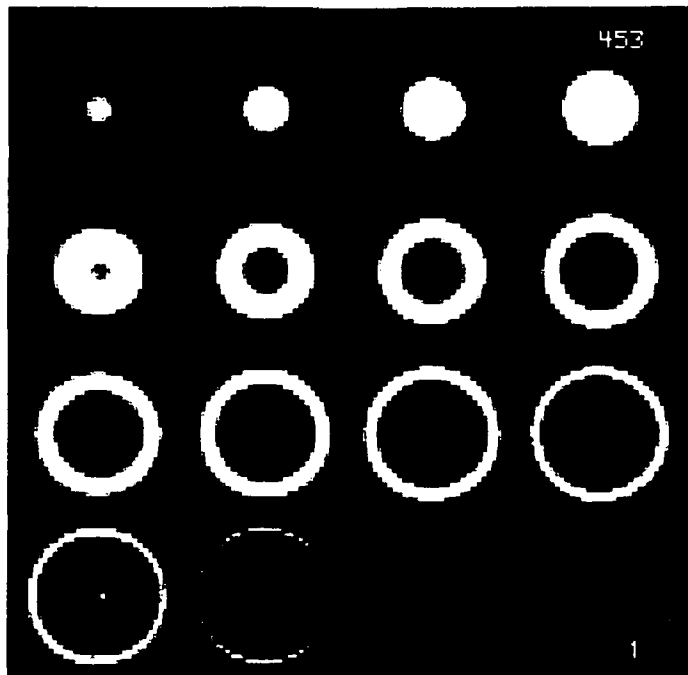


Figure 8: XY slices of 3D flow image of water in 10-mm tube. The top images are individual slices taken perpendicular to Z and the bottom image is a summation of the intensities in the individual slices.

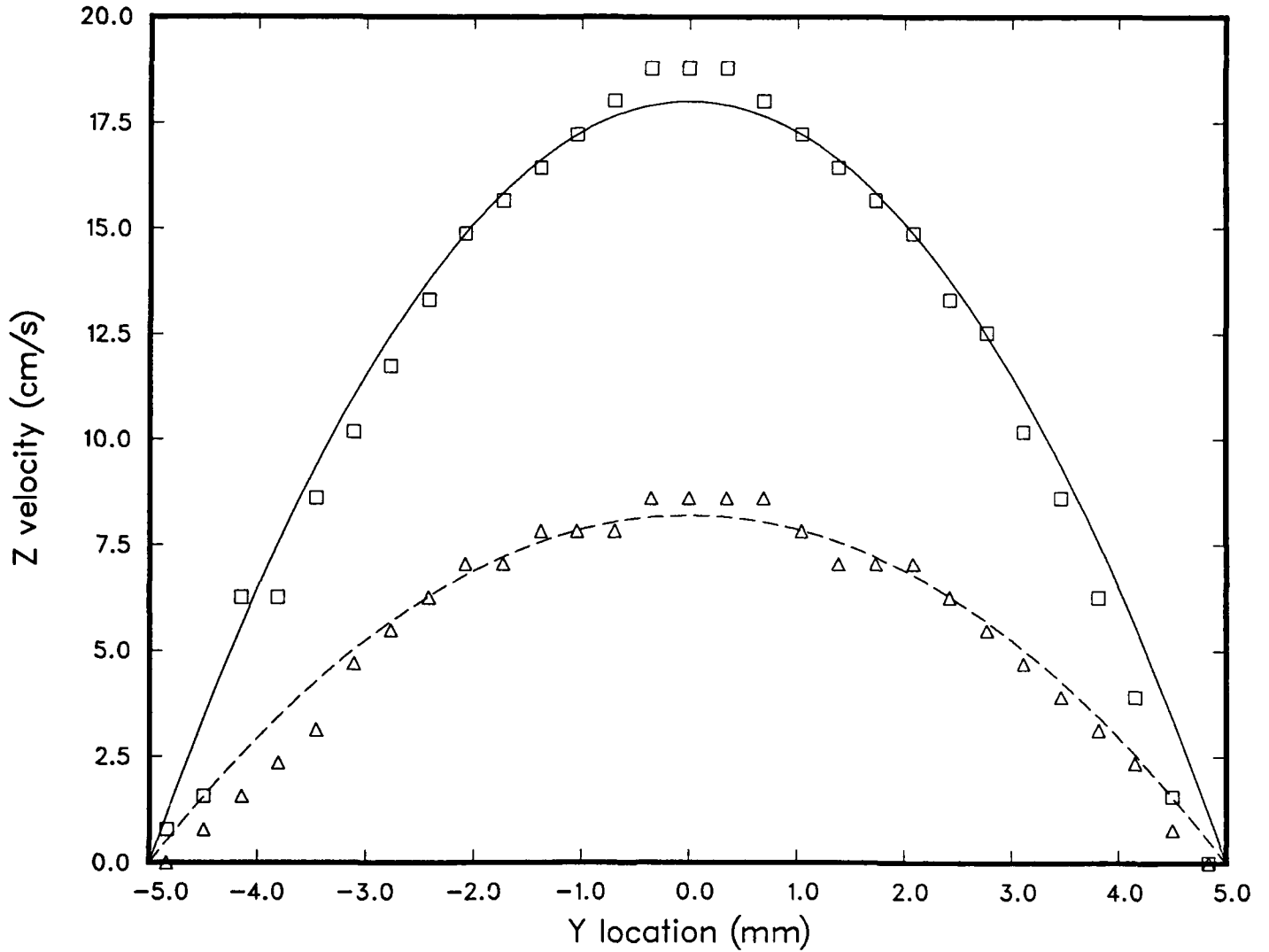


Figure 9: Z velocity profiles along central Y trace of water in 10-mm tube. Data from two different flow rates is plotted along with calculated parabolic curves fitting the data.

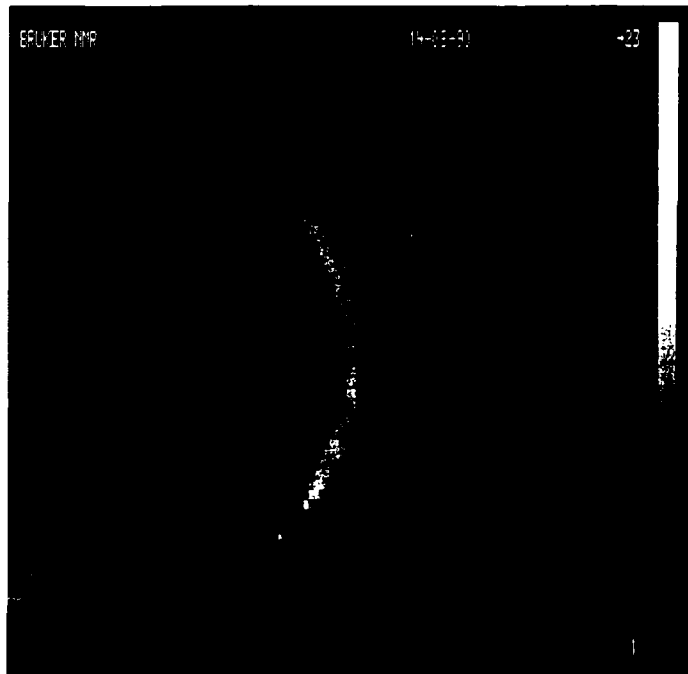


Figure 10: Central XZ and YZ slices of 3D flow image of UCON/20% PMMA suspension in 1-inch pipe.

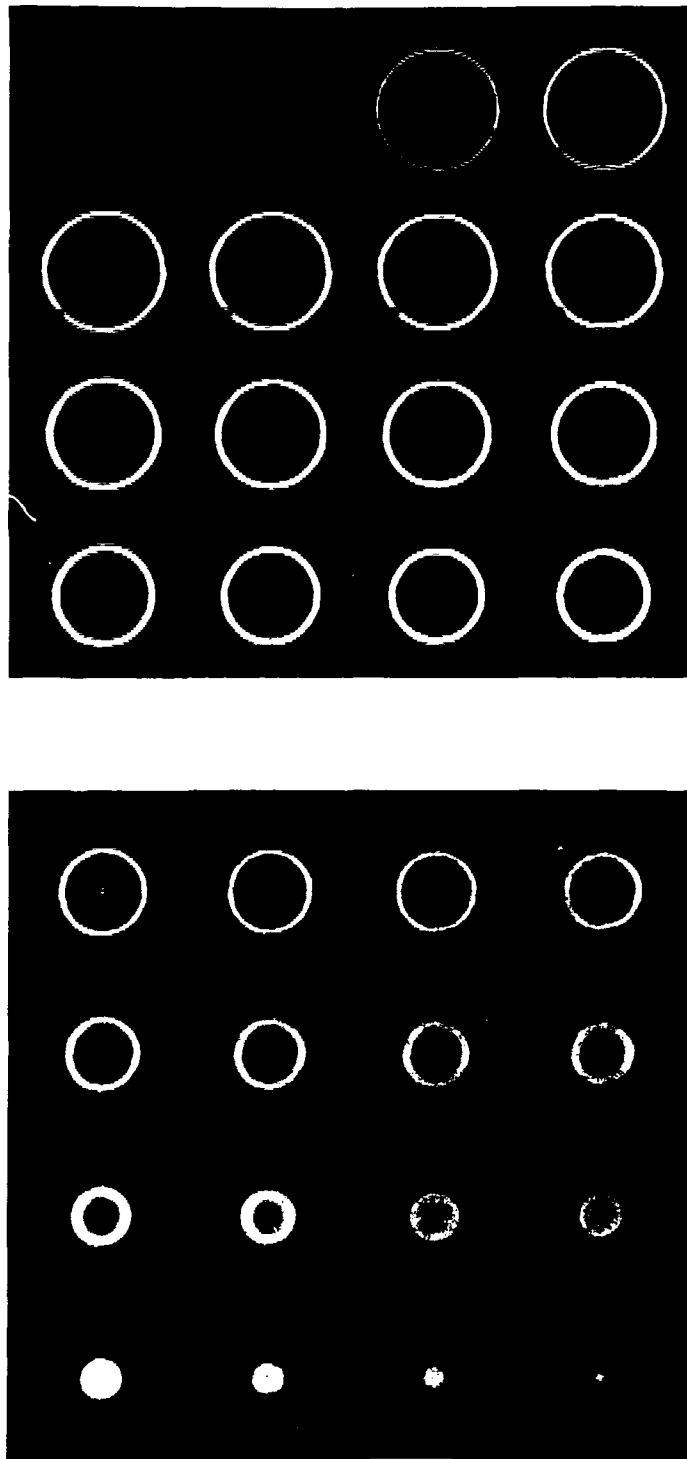


Figure 11: XY slices of 3D flow image of UCON/20% PMMA suspension in 1-inch pipe.

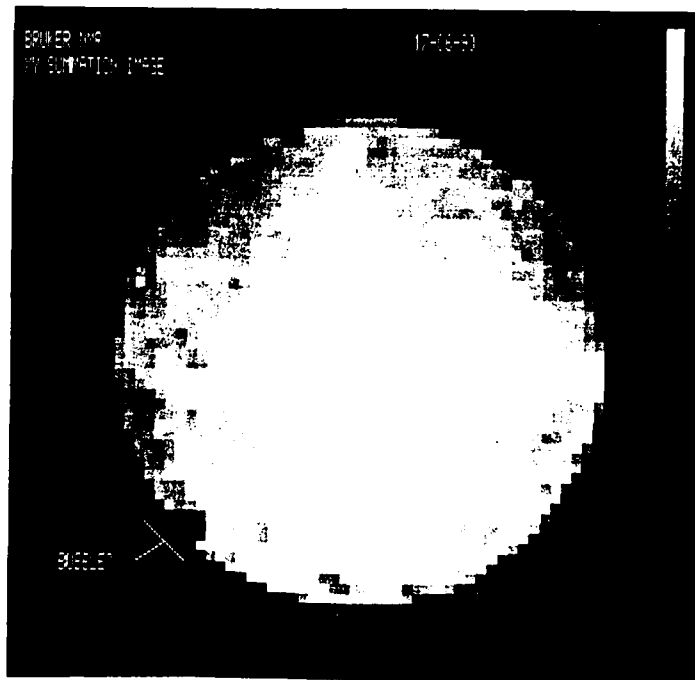


Figure 12: Summation of XY slices of Figure 11.

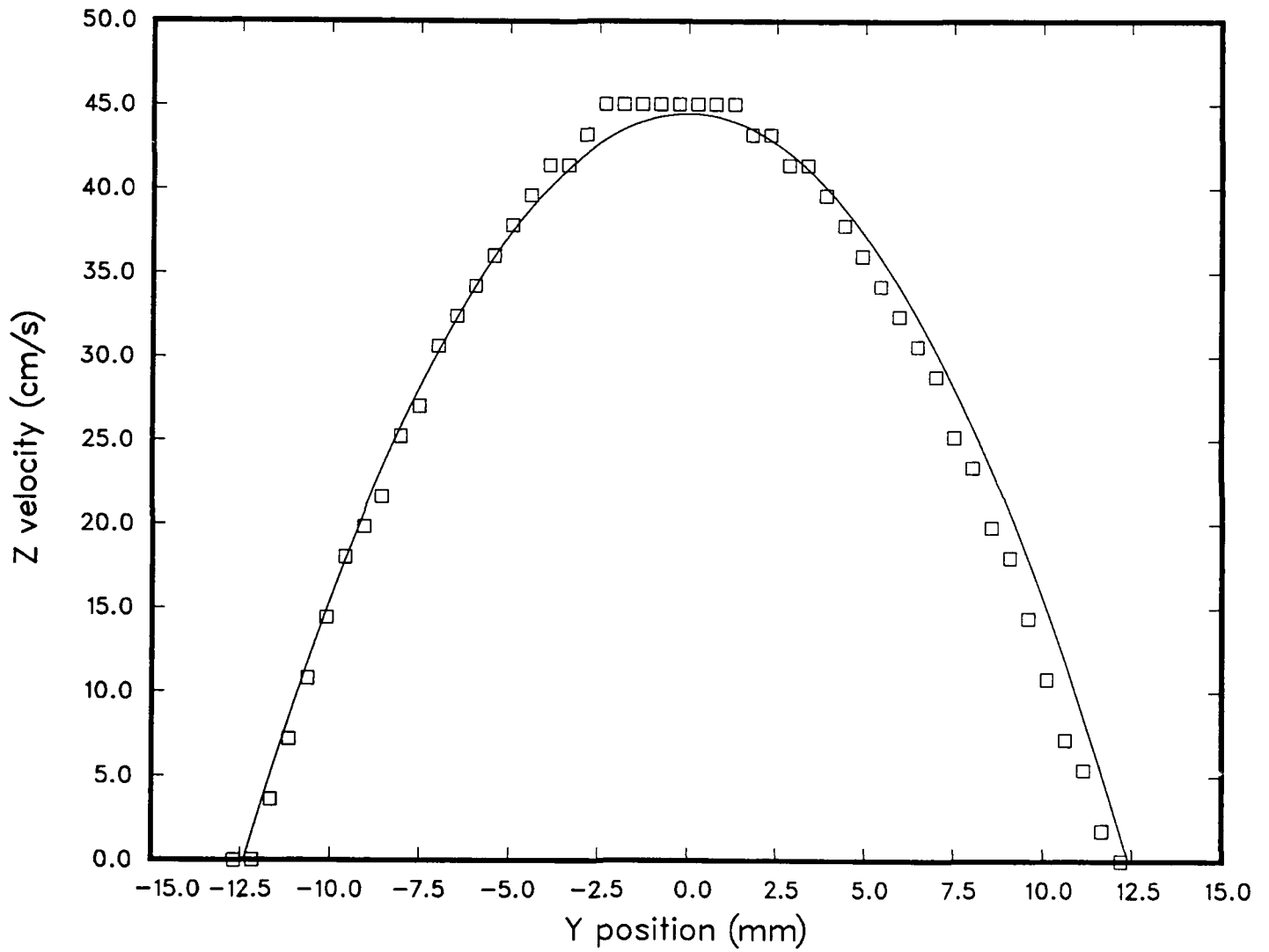


Figure 13: Z velocity distribution for UCON/20% PMMA in 1-inch pipe.

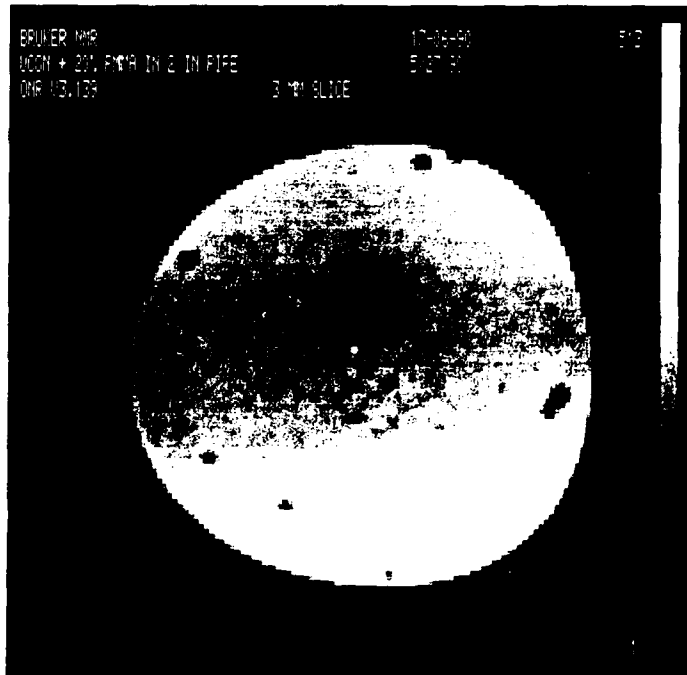


Figure 14: Static image of UCON/20% PMMA in 2-inch pipe.

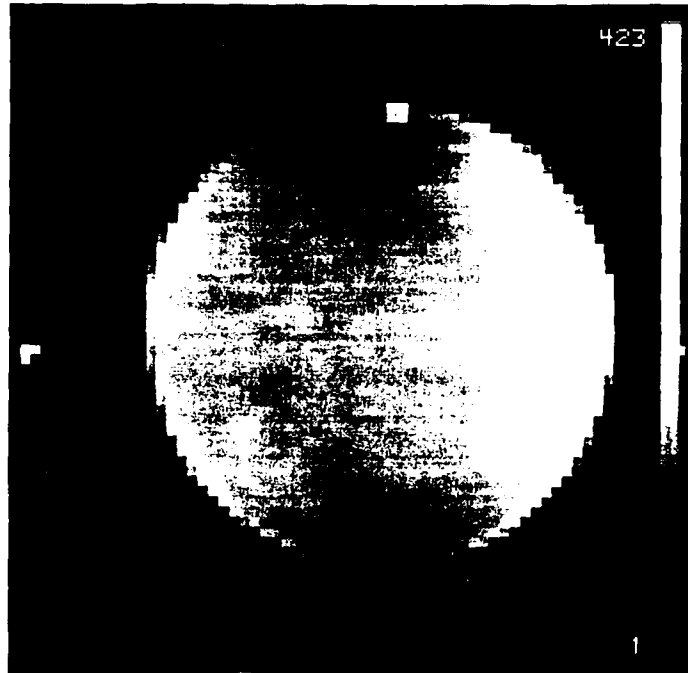


Figure 15: XY summation image of UCON/40% PMMA in 2-inch pipe.

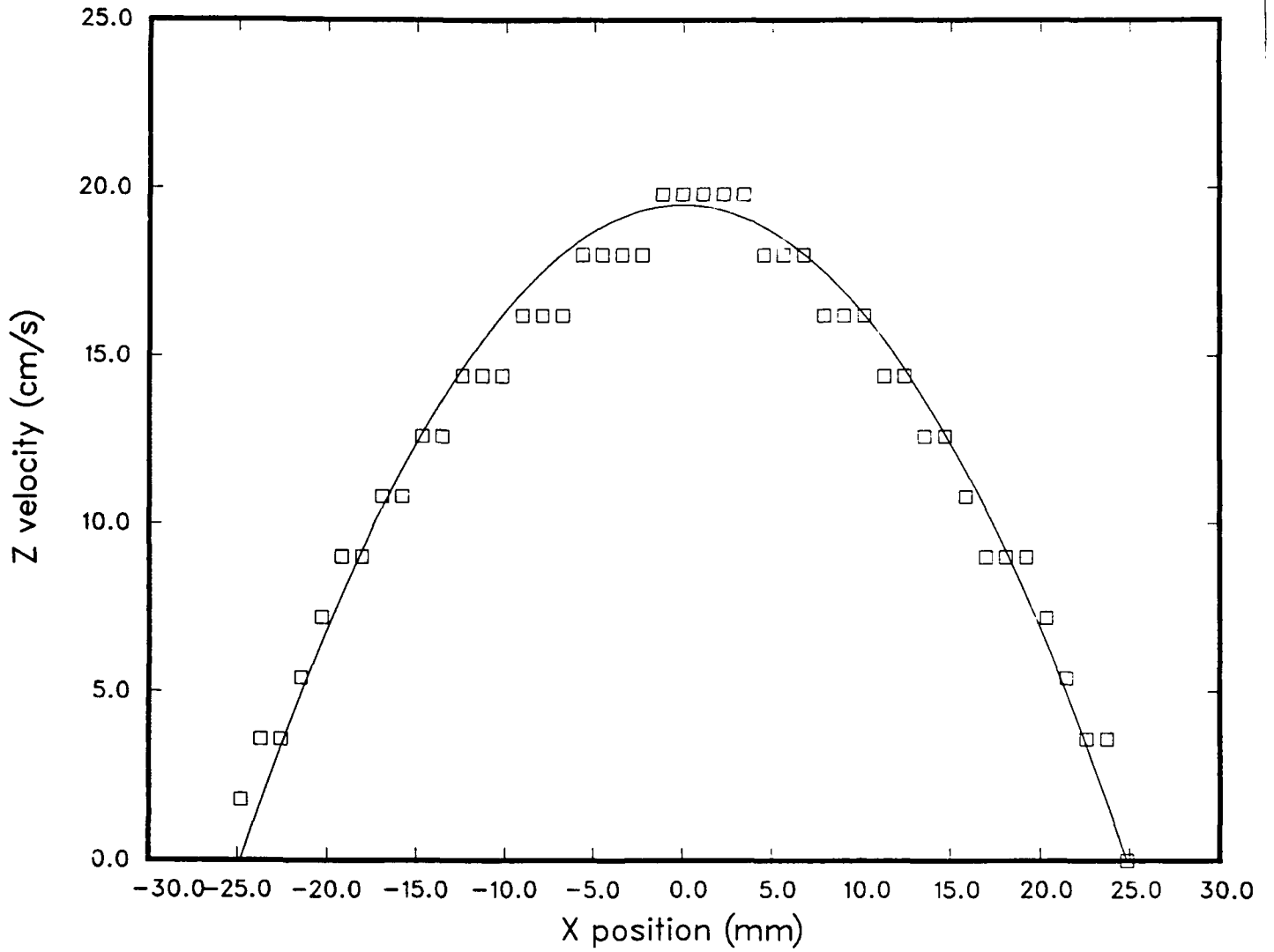


Figure 16: Z velocity profile for UCON/40% PMMA suspension in 2-inch pipe.

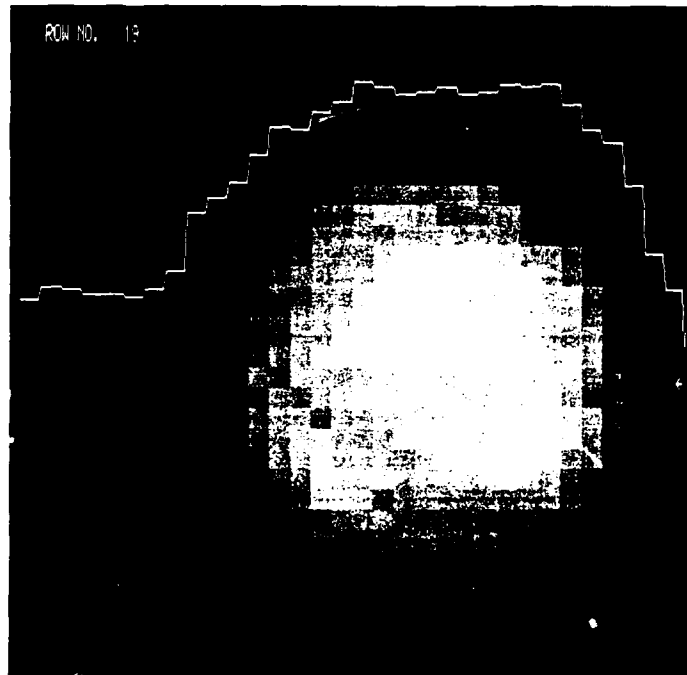


Figure 17: XY summation image of UCON/40% suspension in 0.6-in pipe.

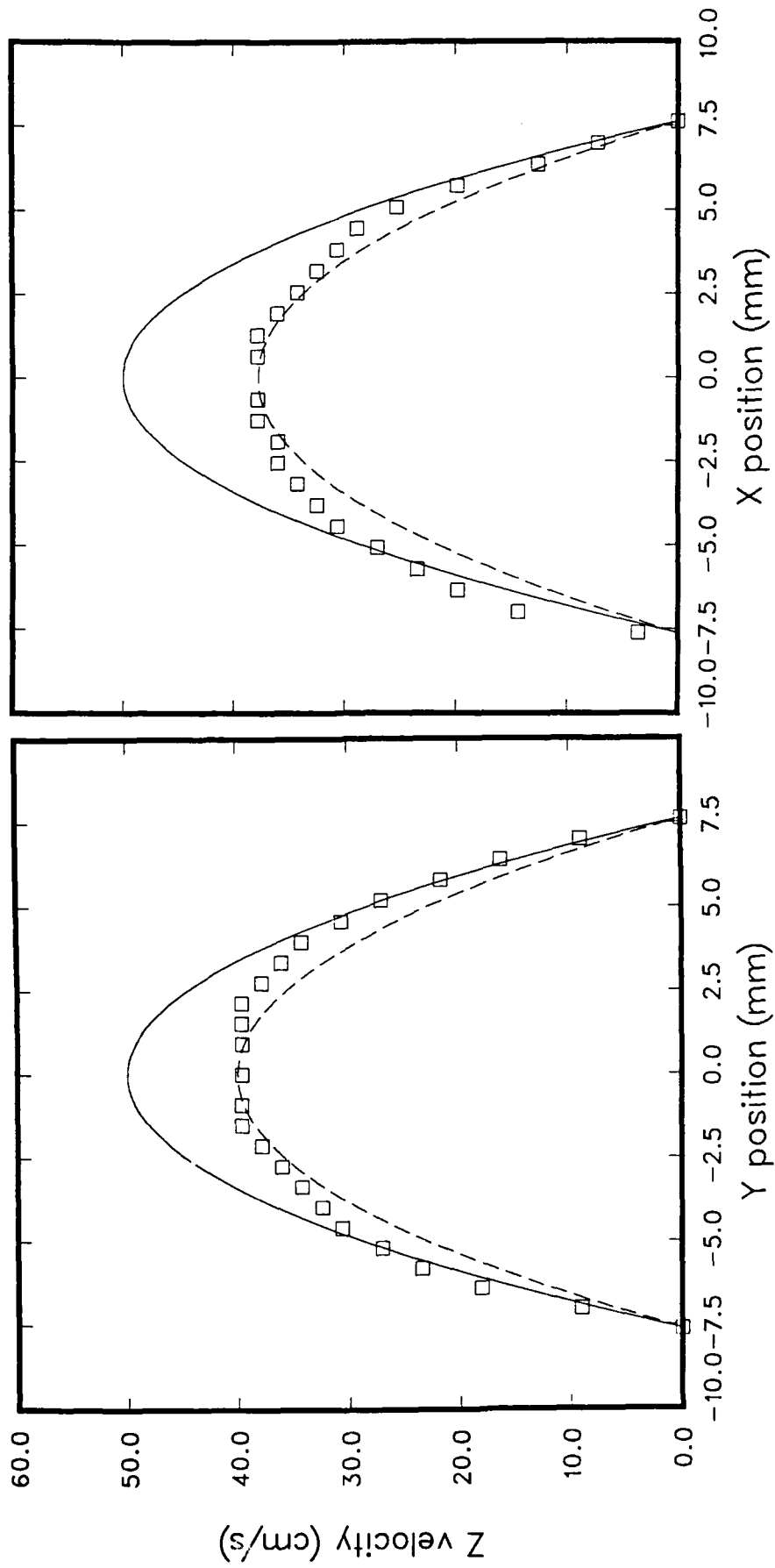


Figure 18: Z velocity profiles along central X and Y traces for UCON/40% suspension in 0.6-inch pipe.

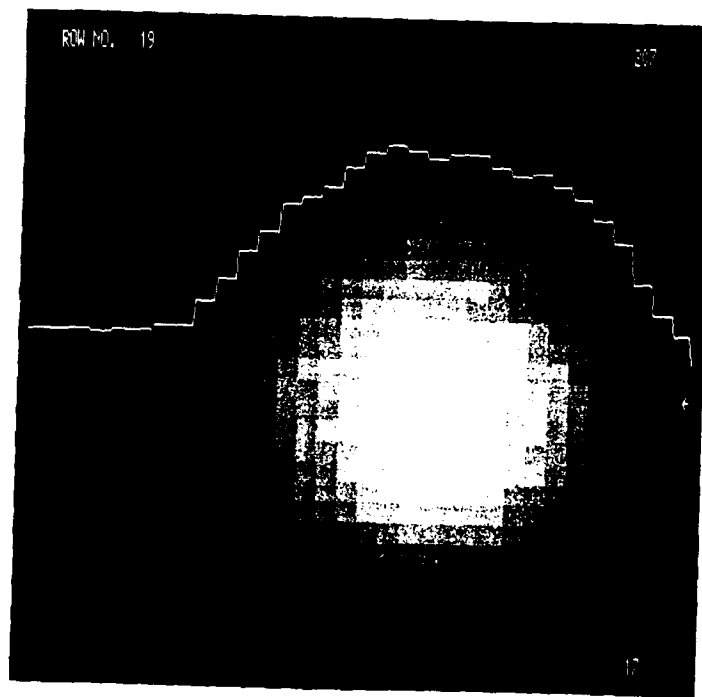


Figure 19: XY summation image of UCON/50% suspension in 0.6-in pipe.

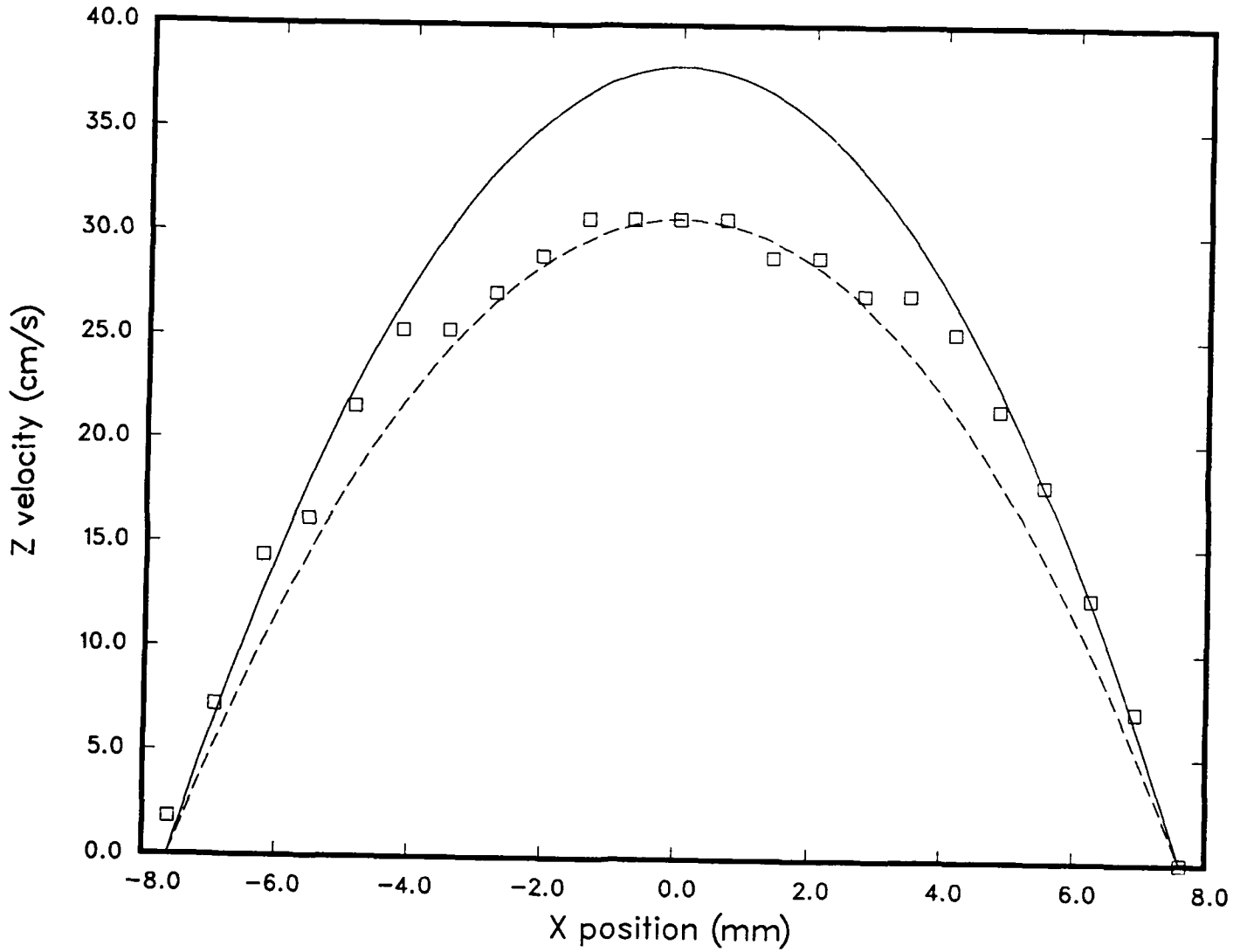


Figure 20: Z velocity distribution along central x trace of UCON/50% suspension.

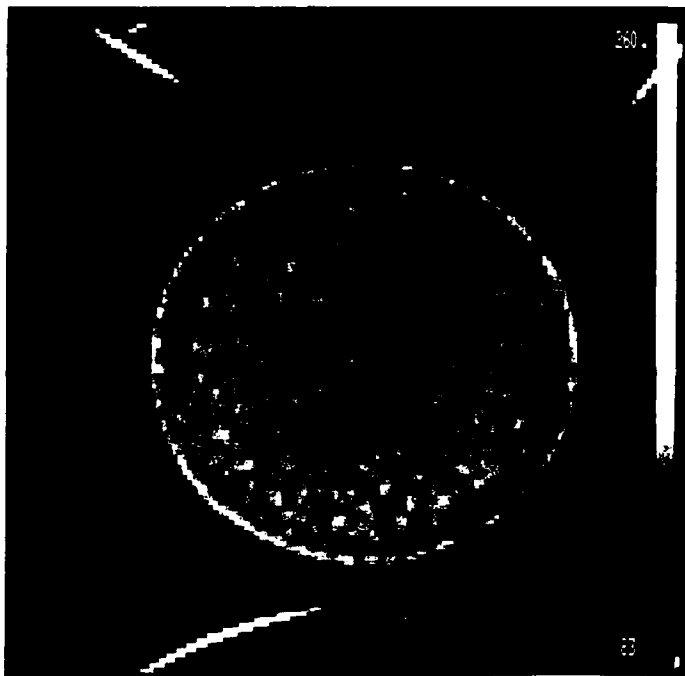


Figure 21: Static XY image of UCON/50% PMMA suspension obtained immediately following cessation of flow.

ATTACHMENT A

"Nuclear Magnetic Resonance Imaging Studies of
Mixing in a Twin-Screw Extruder"

Nuclear Magnetic Resonance Imaging Studies of Mixing in a Twin-Screw Extruder

S. W. SINTON, J. C. CROWLEY, AND G. A. LO

Lockheed Palo Alto Research Laboratory

0/93-50 B/204

3251 Hanover St.

Palo Alto, CA 94304

D. M. KALYON AND C. JACOB

Stevens Institute of Technology

Chemistry and Chemical Engineering

Highly Filled Materials Institute

Castle Point

Hoboken, NJ 07030

INTRODUCTION

The continuous mixing of various ingredients of a multiphase formulation is an important task in polymer processing (1). Mixing operations include the blending of a number of polymeric resins together, reactive processing, and the incorporation of various solid and liquid additives into a polymeric matrix. Some of the commonly used additives include processing aids, cross-linking, foaming and slip agents, stabilizers, antioxidants and pigments. Various fillers and reinforcements are sometimes incorporated to reduce cost or improve the ultimate properties or appearance of the final product.

Among these operations, the compounding of highly filled formulations deserves special attention. For such formulations the loading level is very close to or at the maximum packing fraction (2). They are encountered in various industries including polymeric compounds, ceramics, and energetic materials. The rheology and the ultimate properties of such formulations strongly depend on the conditions and geometry employed during continuous mixing. The mixing conditions control the microstructure of the mixture, which involves the distribution of the liquid and solid components and the physical characteristics i.e., the particle shape and size distribution of the ingredients.

In the continuous processing of highly filled suspensions, on-line quality control becomes very critical. Small changes in the ingredients of the formulation, including changes in the particle size and size distribution of the fillers or reinforcements or the volumetric concentration of the matrix can render a formulation unprocessable (3). Furthermore, lack of adequate mixing or overworking of the formulation can adversely affect the quality of the product. In such continuous processing operations, which may involve single- or twin-screw extruders or single-shaft kneaders run at high production rates, off-line techniques of quality control may lead to very costly waste or recycling problems.

Only a few techniques are currently available for on-line quality control of highly filled suspensions. Included are those techniques which characterize the rheological behavior or the chemical composition of the compound and surface-based methods such as fluorescence and FTIR. Techniques capable of determining the three-dimensional spatial distribution and characteristics of opaque mixtures would be particularly valuable. In this last category nuclear magnetic resonance imaging (NMRI) has been identified as a new technology with particular promise. In this paper, we report on two novel studies of continuous polymer extrusion using NMRI. The first study involves the determination of the goodness of mixing of a solid filler into a polymer melt. The second study addresses the patterns of flow developed in a twin-screw extruder. Our results show the potential of NMRI and represent the precursors

of revolutionary new techniques which can significantly change the on-line process capabilities of many industries, including the rapidly growing polymer-based processes.

NMRI ANALYSIS OF GOODNESS OF MIXING OF MULTIPHASE COMPOUNDS

The first study involves a simple formulation consisting of a liquid polymer (acrylonitrile terminated poly(butadiene) or PBAN) and a solid filler, in this case ammonium sulfate (AS) powder. The mixing task at hand involves the homogeneous distribution of AS in the PBAN matrix. The attritive changes in the shapes and sizes of ultimate particles and agglomeration or deagglomeration of the solid components also need to be monitored. The loading levels considered are 60-70 percent by volume, and are thus in the highly filled range.

The traditional approach to characterizing the goodness of mixing of such a formulation involves the collection of a sample from the die or from a port of the extruder and its labor intensive analysis at the lab. Typically this analysis may consist of scanning electron microscopy of the samples of the mixture. Computerized image analysis (4,5) can generate quantitative information on the distribution of the phases but requires clearly delineated intensity characteristics for distinguishing between different phases. This may require the dissolving, leaching, etc. of one or more of the phases (5). Furthermore, while the distribution of phases can be determined by SEM at the particle level, information about mixing at larger length scales is difficult to obtain by this method.

Equipment and Procedures

The PBAN and ammonium sulfate formulation described earlier was mixed in a 50.8 mm fully intermeshing, co-rotating twin-screw extruder. The extruder had a clam-shell design, splittable barrel. An Acrison loss-in-weight feeder was used to feed in the ammonium sulfate and a Zenith gear pump to feed the PBAN. Upon achieving steady state, the extruder was brought to a dead-stop, the barrel opened and samples from various locations were collected. The configuration of the screw and the locations where samples were taken are shown in Figure 1. These samples were then placed in standard 10-mm sample tubes and subjected to NMR imaging analysis.

NMR imaging was done on a commercial instrument fitted with an extra wide bore (15 cm) superconducting solenoid magnet. The magnetic field strength was 4.7 T, corresponding to a proton resonance frequency of 200 MHz. The probe circuit used in this work was tuned to the proton resonance. Thus, the images discussed below involve the distribution and magnetic resonance properties of hydrogen. The imaging procedures used and typical instrument parameter settings are described elsewhere (6).

Results for PBAN/AS Mixtures

Figure 2 shows the proton NMR images of four PBAN/AS samples from the locations indicated in Figure 1. Images were obtained by electronically selecting a slice 0.25 mm thick and perpendicular to the axis of the sample tube. Each image is made up of 128 X 128 pixels with a resolution in the image plane of about 100 $\mu\text{m}/\text{pixel}$. The imaging parameters were such that the hydrogen nuclei of the solid AS particles do not contribute to the image. Thus, pixel intensity in this case corresponds to the local concentration of PBAN polymer. Dark areas are evident in the images and are particularly noticeable in the images of samples taken from regions closest to the screw feed (top row of Figure 2). These dark features represent clumps of AS which have not been broken up and mixed into the PBAN. It is evident that the mixture becomes more homogeneous further down the screw since the bottom images in Figure 2 appear to have more uniform intensities than the top images.

This last statement is supported by a somewhat more quantitative view of the degree of mixedness as determined by NMRI. Figure 3 shows histogram plots of each of the four images of Figure 2. These plots show the relative incidence of each gray level in an image. Each histogram in Figure 3 consists of two major peaks. The largest peak comes from those low-intensity pixels falling outside the circular PBAN/AS shape. We refer to this as the "noise" peak since its shape depicts the distribution of noise amplitude in that portion of the image outside of the object of interest. The peak at higher intensities is called the "object" peak since it arises from pixels within the object. The separation between noise and object peaks is a measure of the signal-to-noise ratio of the image. The extent to which the object peak is broader than the noise peak is an indication of the presence of true gray-scale features within the object. Thus, as the material became better mixed by the break up and dispersion of AS clumps, the variance of the object intensity distribution decreased as observed in Figure 3. This result clearly demonstrates that NMRI can give valuable information on the quality and mechanisms of mixing in highly filled polymers. Other, more sophisticated, statistical techniques such as spatial autocorrelation are also being developed for this application.

NMRI STUDY OF FLOW DYNAMICS IN A CONTINUOUS MIXER

The purpose of this study was to define the potential of NMRI for investigations of the flow patterns and dynamics of distributive mixing processes in extrusion. Previous work in this area has usually involved ideal systems containing well defined minor and major components which can be easily distinguished. This allowed the distribution of the components after some degree of mixing to be determined. Examples include the use of white and colored clay (7), pigmented polyethylene granules (8), and black and white silicone rubbers (9). We chose to work with a plasticized thermoplastic elastomer (TPE) system which is pigmented with trace amounts of zinc oxide and carbon black. This choice was made to maintain commonality with earlier work (4) in which coloration of the TPE was necessary to allow visualization of the flow patterns and because of the special effect carbon black has on NMR images (discussed below).

Equipment and Procedures

The TPE system consisted of a styrene ethylene/butylene styrene block copolymer with white mineral oil as a plasticizer. The plasticizer/polymer weight ratio was four. The plasticized TPE was compounded with either 4% by weight zinc oxide (white) or 1-3% carbon black (black). Rheological characterization of this material has been presented elsewhere (4). The twin-screw extruder was first loaded with molten, white TPE which was then frozen in place once the screw cavity was filled. The barrel was then opened and wedges of TPE were cut out. The holes left behind were then completely filled with black TPE. The barrel was closed and heated above the TPE melt temperature once again. After a small number of turns (~10) the barrel was cooled, re-opened, and samples were excised from selected locations. Typical sample dimensions were 10-25 mm. Digital image analysis of these samples has been described elsewhere (4). The same samples were then subjected to NMR imaging by the methods described above.

NMRI Results on Filled TPE Samples

Figures 4 and 5 shows two images of one TPE sample taken along orthogonal planes. A photograph of this sample appears as Figure 6. Zinc-oxide-filled regions are white in the NMR images while carbon-black-filled regions and voids are either darker or completely black. Contrast between the two types of

TPE regions exists even though their hydrogen density is nearly identical. Therefore, unlike the PBAN/AS case, there must be some source of contrast other than polymer concentration. The answer is found in the high concentration of unpaired electrons in the carbon-black particles. These electron sites cause the magnetic resonance of nearby protons in the TPE matrix to rapidly decay relative to the NMR response of protons in the zinc-oxide regions. Such differential relaxation effects (" T_2 weighting") are well known in NMRI and provide a useful means of resolving features when nuclear density is nearly constant. T_2 -weighted NMR imaging can conceptually lead to a determination of the three dimensional flow patterns developed in a complex geometry such as an extruder without the use of a perturbing probe.

Figure 7 shows another NMR image of a TPE sample taken from a separate run. This time the carbon black concentration was on the order of 1%, and the sample was cut from a different location in the extruder. The decreased concentration of electrons results in a decrease in the contrast between the two types of pigmented regions. In Figures 4 and 5 it is difficult to distinguish voids from carbon-black regions since both map to the lowest gray levels. This is not a problem in Figure 7 where voids (bubbles) are definitely the darkest features within the object. Although not shown here, image contrast for this material can be conveniently adjusted by varying the imaging parameters which control the relative T_2 weighting factors. A photograph of this TPE sample is shown in Figure 8. The agreement with Figure 7 is obvious, as well as the extra features evident in the NMR image.

CONCLUSIONS

Various techniques are currently available to characterize the goodness of mixing of highly filled polymer suspensions. However, generally these techniques are off-line and are labor intensive. In this field the large potential of nuclear magnetic resonance imaging, NMRI, remains untapped. NMRI is a non-intrusive, non-invasive, three-dimensional technique which can be used to identify (potentially on-line) the spatial distribution, chemical nature, and physical characteristics of various components in highly filled materials. Typical results obtained on samples collected from various down-channel locations of a twin-screw extruder have revealed that the degree of mixing of the ingredients can be distinguished. The dynamics of flow patterns within the complex extruder cavity.

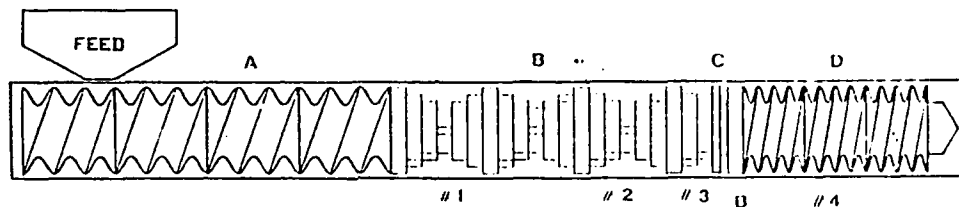
NMRI should be compared with other potential on-line techniques such as densitometry and X-ray imaging. Although sometimes useful, density measurements usually do not provide spatially resolved information. Also, density alone may not give a sensitive enough measure of composition when several components having similar individual densities are mixed. For highly filled polymer suspensions such as those considered in this study, X-ray is primarily sensitive to the solid component and so provides complementary information to NMRI. The next decade will likely witness many new applications of NMRI for on-line analysis for quality control and fundamental studies of filled, highly filled and reinforced polymeric compounds.

ACKNOWLEDGMENTS

This research was part of separate contracts at Lockheed (N00014-86-C-0724) and Stevens (N00014-86-C-0620) supported by SDIO/IST and managed by the Office of Naval Research. Some of the mixing and characterization experiments were carried out by Mr. H. Sangani and Dr. S. Dey of SIT.

REFERENCES

1. D. Kalyon, in *Encyclopedia of Fluid Mechanics*, Volume 7, N. Chermisinoff, Ed., pp. 887-926, Gulf Publishing Company (1988).
2. U. Yilmazer and D. Kalyon, *J. Rheology*, in print (1989).
3. U. Yilmazer, C. Gogos, and D. Kalyon, *Polym. Comp.*, **10**, 242 (1989).
4. D. Kalyon and H. Sangani, *Polym. Eng. Sci.*, **29**, 1019 (1989).
5. D. Kalyon, A. Gotsis, U. Yilmazer, C. Gogos, H. Sangani, B. Aral and C. Tsouglou, *Adv. Polym. Techn.*, **8**, 337 (1988).
6. J. M. Listerud, S. W. Sinton, and G. F. Drobny, *Anal. Chem.*, **61**, 23A (1989).
7. K. Hall and C. Godfrey, *Inst. Chem. Eng.*, **10**, 71 (1965).
8. M. Goekbora, *Ph.D. Thesis*, University of Bradford, U.K. (1981).
9. C. Howland and L. Erwin, *SPE ANTEC Technical Papers*, **29**, 113 (1983).

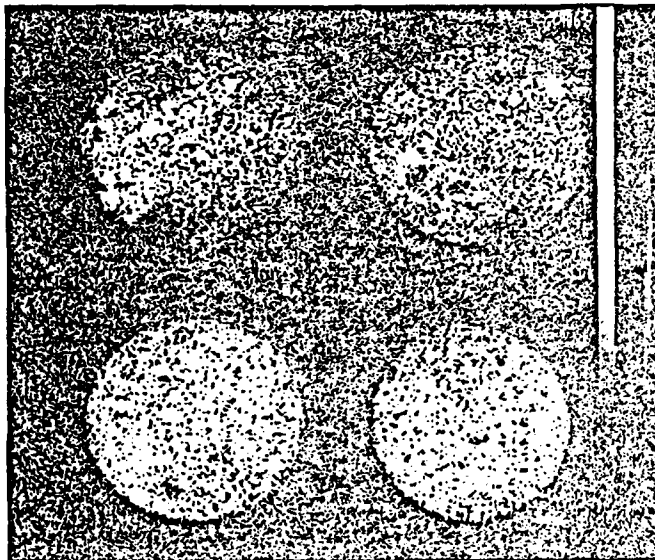


TYPICAL SCREW CONFIGURATION USED IN THE EXPERIMENTAL SETUP

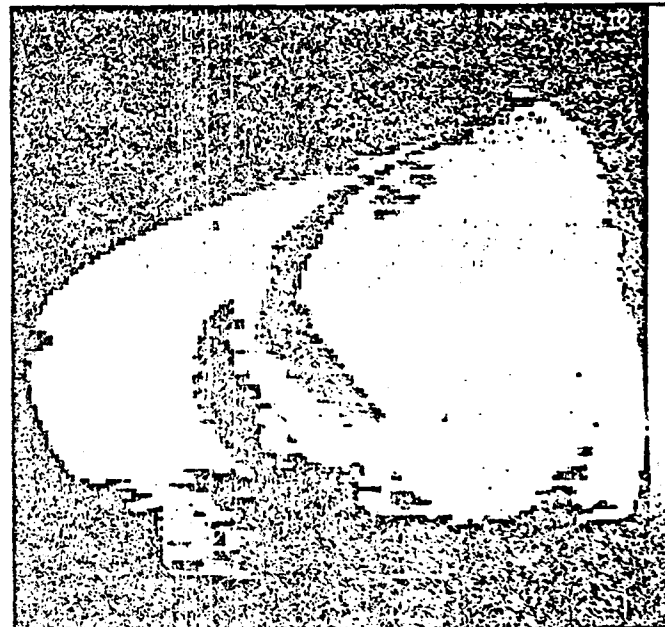
Screw Elements

- A: regular, forward, double flighted screw elements with 50.8 mm pitch.
- B: 21 kneading disks, staggered at 60° forward
- C: neutral disk.
- D: regular, forward, single flighted screw elements with 12.7 mm pitch.

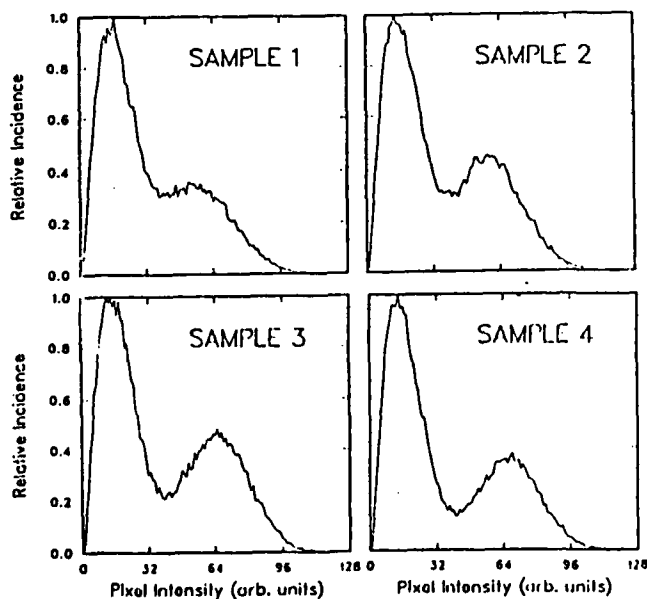
1. Configurations of the screw extruder. Locations where samples were taken for NMRI analysis are indicated by the numbers.



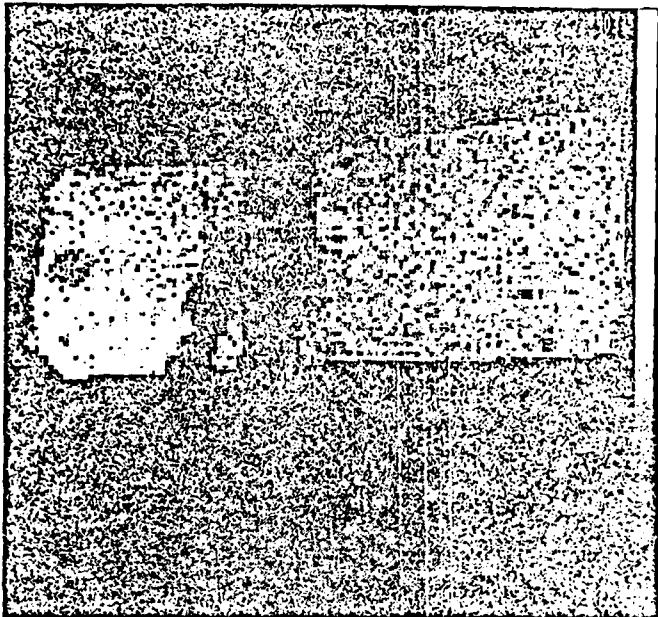
2. NMR images of PSAN/AS samples. The order of the samples is from the feed to die end of the extruder (see Figure 1) going from left to right across the top row and again across the bottom row.



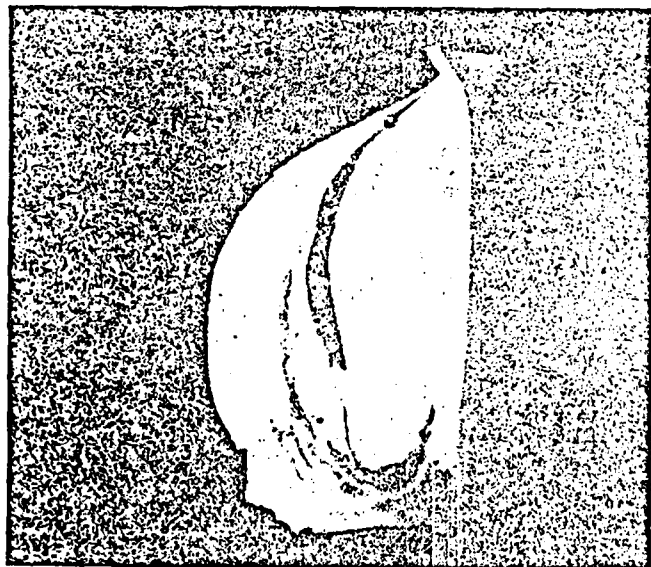
4. NMR image of pigmented TPE sample excised from extruder after screw rotation. This image is of a .5 mm slice selected through the center of the sample and running parallel to the major axes of the sample. Note that the vertical dimension of this image has been compressed to more completely fill the view.



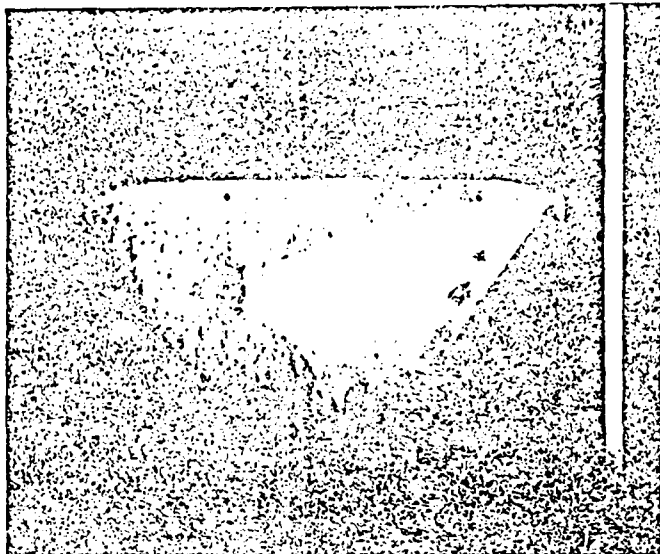
3. Pixel intensity histograms of images in Figure 2.



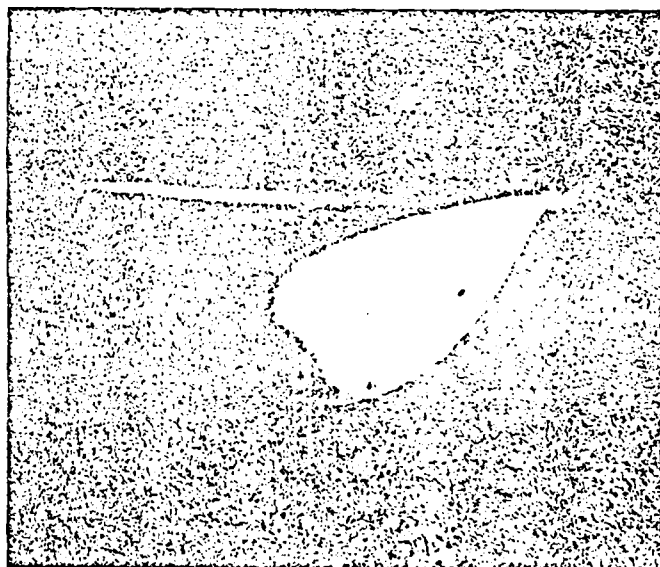
5. NMR image of TPE sample #3 in Figure 4 except along a plane perpendicular to the image plane of that figure. Slice thickness = 1 mm.



6. Photograph of the TPE sample imaged in Figures 4 and 5. Dimensions of the sample are 22 x 10 x 6 mm.



7. NMR image of second pigmented TPE sample. This image is of a 1-mm slice taken through the center of the object and parallel to the major sample dimensions.



8. Photograph of sample imaged in Figure 7. Sample dimensions are roughly 25 x 11 x 3 mm.

ATTACHMENT B

"Stokesian Dynamics Simulation of Polyether-coated
Particles in a Shear Flow"

AV 2176
A15-4

Stokesian Dynamics Simulation of Polyether-
Coated Particles in A Shear Flow

M. Seel, D.T. Wadiak*,
A.B. Kunz and S.E. Hill

Department of Physics
Michigan Technological University
Houghton, Michigan, 49931

* Lockheed Palo Alto Reasearch Laboratory
Reseach and Development Division
Lockheed Missiles and Space Co., Inc.
Palo Alto CA 94304

RECEIVED 9 JANUARY 1990

~~ABSTRACT~~

The development of a Lennard - Jones type polymer - polymer interaction model is described, appropriate for monolayer polymer coatings on spherical solid particles suspended in a polymer fluid. This model is appropriate for polymer - coated particles interacting at very close proximity (Angstroms). These molecular forces, derived from ab initio calculations for polyoxymethylene - polyoxymethylene interactions are added to the hydrodynamic forces of a Stokesian Dynamics simulation in order to estimate the effect of a polymer coating on the behavior of suspended particles under sheared conditions. The relation between suspension microstructure, shear velocity and their time evolution are studied in molecular dynamics - like simulations.

I. INTRODUCTION

The bulk rheological properties of particle filled polymer suspensions such as propellant and explosive mixes are influenced by particle-particle interactions. It is known that the rheological behavior of these mixes may affect the quality of the cured product in terms of mechanical properties, as well as the ability to mix and process these materials prior to cure. The particle - particle interactions are dominated by hydrodynamic forces at large and intermediate particle separations, corresponding to dilute and intermediate particle concentrations. In concentrated suspensions, as the probability of very small (1-10's of Angstroms) particle separations increases, non-hydrodynamic forces such as van der Waals forces between the surfaces of the particles can play a dominant role in the formation of particle clusters and agglomerates.

To understand the rheology of particle - filled polymeric suspensions on an atomistic or molecular level several types of microscopic interactions have to be considered. First the elastic properties of a single polymer chain must be understood. Second, the fundamental interaction of a polymer chain with a polymer chain has to be characterized. Third, the mechanistics of the polymer - particle interactions are needed, and finally the mechanistics of the polymer -

wall interaction to describe a real fluid in a confined flow. In a previous paper [1] the results of an ab initio Hartree-Fock model study of the first three types of interactions are reported using polyoxymethylene as the simplest polyether and ammonium perchlorate and aluminum as particles.

In order to predict macroscopic properties like shear viscosity, one has to bridge the gap between the quantum chemistry computations and computational fluid dynamics. The molecular - dynamics - like approach developed by Bossis, Brady and D. Lofsky [2-5], called Stokesian Dynamics, is the method chosen for the present investigation since it allows the addition of external, non - hydrodynamic forces in a straightforward manner. The aim of the paper is to derive an interaction potential between micron - sized spheres from quantum chemical results and to study the effect of these additional forces. Using molecular forces and hydrodynamics is to join physics on two different length scales [3] and has to be carefully investigated. Therefore, we have not included Brownian motion or additional external forces such as surface roughness to keep the number of parameters as small as possible. On the other hand, the rapid advances in computational resources are such that the fundamental atomistic level of many empirical factors can be investigated and an intergrated computer model can be developed.

II. METHOD

A. General Method

The Stokesian Dynamics (SD) method [2-5] is briefly summarized here in order to introduce its elements. SD is a generalized computational method that describes the time evolution of any number of solid, uniformly sized spherical particles interacting in a Newtonian suspending medium of constant density, viscosity and temperature, and externally influenced by wall shear or other forces such as gravity. The governing equation describing the particle velocities is written in matrix form:

$$R \cdot U^* + \phi : E + F_p = 0 \quad (1)$$

where U^* is a vector of dimension $6N$ (for N particles) containing the translational and rotational particle velocity component relative to the bulk fluid translational - angular velocity evaluated at the particle center, F_p is the nonhydrodynamic force such as electrostatic repulsion or Lennard-Jones (L-J) interactions. This equation is valid for a small particle Reynolds number, a large appropriately defined Peclet number,

in the absence of Brownian motion, and for particles undergoing a bulk linear shear flow characterized by a constant symmetric strain rate tensor E and constant vorticity. The matrix R is the grand resistance matrix and is dependent upon the instantaneous configuration of all particles. R relates the force/torque exerted by the suspending fluid on all N particles relative to the fluid. The shear resistance matrix ϕ gives the force torque on a particle in the suspension due to the bulk shear flow. If we solve for particle velocities, Equation (1) becomes:

$$U^* = -R^{-1} (\phi:E + F_p) \quad (2)$$

where R^{-1} is the inverse of R . R , ϕ and F_p are all configuration dependent, and are thus functions of time and require updating periodically or at each time step in a computational simulation. F_p is any appropriate nonhydrodynamic force, for which we have chosen to examine the L-J interaction. Inclusion of the L-J force is straightforward in Equation (2) as F_p appears separately from the hydrodynamic force $\phi:E$ and only requires a description of the force-separation distance relationship be evaluated for each particle pair separation distance and added to the hydrodynamic force at any time step. Simulations were carried out by using J.F. Brady's computer code SDWL (for Stokesian Dynamics with Walls).

B. Lennard - Jones Interaction Between 2 Spheres Due to Adsorbed Material

In a previous quantum mechanical study [1] we investigated the interaction between polyoxymethylene (POM) polymer chains. An attractive minimum of 1.3 kcal/mol per unit cell was found in the potential energy curve for two chains for a chain - chain separation of 4.3 Å, in reasonable agreement with the experimental value of 4.43 Å for a hexagonal unit cell. Particulate aluminum is a common constituent of propellants, and it was found that coating of aluminum particle surfaces by POM units is possible. Therefore, in addition to hydrodynamic interactions, polymer - covered particles in a suspension will interact through weak van der Waals-like forces for separations on the order of Angstroms.

The classical Derjaguin - Landau - Verwey - Overbeek (DLVO) picture [6,7] of forces between colloidal particles is a linear superposition of attraction due to London dispersion forces and repulsion caused by electrical double layers surrounding the particles. We will use a Lennard-Jones 6-12 potential for the interaction between two polymer units:

$$V(r) = -4\epsilon \left[\left[\frac{\sigma}{r} \right]^6 - \left[\frac{\sigma}{r} \right]^{12} \right] \quad (3)$$

and derive the force between spherical particles covered by polymer units using the Derjaguin procedure [8]. This method allows us to calculate the interaction between two spheres if the interaction of two infinitely large parallel plates of the same material is known. As a first approximation the interaction is assumed to be pairwise additive. Consider then, one polymer unit opposite to an infinitely large plate assumed to be covered by a monolayer of polymer. The L-J force is then found by adding all force components exercised by the polymer units of the plate surface, in a direction perpendicular to the surface plane.

The force component between a pair of polymer units is (see Figure 1):

$$f(r) = -24\epsilon \left[\frac{\sigma^6}{r^7} - 2 \frac{\sigma^{12}}{r^{13}} \right] \cos\phi \quad , \quad \text{where } \cos\phi = R/r. \quad (4)$$

If q denotes the number of polymer units per unit surface area, the number of polymer units in a ring with radius ρ is $2\pi q\rho d\rho$. The total force between the reference polymer unit and an infinitely large plate at a distance R is then:

$$\tilde{f}(R) = -48\pi q\epsilon \int_0^\infty \left[\frac{\sigma^6}{r^7} - 2 \frac{\sigma^{12}}{r^{13}} \right] \frac{R}{r} \rho d\rho . \quad (5)$$

As $r^2 = R^2 + \rho^2$, we obtain

$$\bar{f}(R) = -48\pi q\epsilon R \int_0^{\infty} \left[\frac{\sigma^6}{(R^2 + \rho^2)^4} - 2 \frac{\sigma^{12}}{(R^2 + \rho^2)^7} \right] \rho d\rho \quad (6)$$

$$= -8\pi q\epsilon \left[\frac{\sigma^6}{R^5} - \frac{\sigma^{12}}{R^{11}} \right] \quad (7)$$

Since the surface of plate 1 also contains q polymer units per unit area, the total force per unit area between two infinitely large plates separated by R is:

$$F(R) = -8\pi q^2\epsilon \left[\frac{\sigma^6}{R^5} - \frac{\sigma^{12}}{R^{11}} \right] \quad (8)$$

Derjaguin's procedure is applicable when the range of interaction is much smaller than the particle radius which is satisfied for concentrated suspensions with particle radii in the micron range. The spheres are thought of as split into parallel lamellae of area $2\pi h dh$ (see Figure 2), which are considered to interact as if they were flat plates [6-8]. Each pair of lamellae contributes to the L-J force an amount equal to $2\pi h F(R) dh$, $F(R)$ being the force per unit area of two parallel plates at distance R , h being the distance of the lamella considered from the axis of symmetry. The total L-J force is then found by integrating over the surface of the spheres. With the assumption that the interaction range is much smaller than the sphere radius, the contributions of layers far from the axis are unimportant, and the upper

limit of integration becomes immaterial, usually chosen as infinity.

With:

$$\frac{R - R_0}{2} = a - (a^2 - h^2)^{1/2}, \quad (9)$$

$$2hdh = a(1 - (h^2/a^2))^{1/2} dR,$$

which can be approximated by adR , we obtain for the L-J force between two spheres having a radius a and being separated by a distance R_0 :

$$F(R_0) \sim \pi a \int_0^\infty F(R) dR = -4\pi^2 q^2 \epsilon a \left[\frac{\sigma^6}{2R_0^4} - \frac{\sigma^{12}}{5R_0^{10}} \right], \quad (10)$$

or, for the potential energy:

$$V(R_0) = -\frac{4}{3}\pi^2 q^2 \epsilon a \left[\frac{\sigma^6}{2R_0^3} - \frac{\sigma^{12}}{15R_0^9} \right] \quad (11)$$

C. Approximate L-J Interaction for SD simulations

The parameter ϵ and σ in the 3-9 potential describing the surface interaction between two spheres are determined by the ab initio values for the equilibrium position r_e and the well depth at r_e , obtained for the 6-12 potential of two polymer unit cells (Equation (3)):

$$\sigma = \frac{r_e}{(2)^{1/6}} = \frac{4.43}{(2)^{1/6}} \text{ \AA} \sim 4 \times 10^{-10} \text{ m}, \quad (12)$$

$$\epsilon = 1.3 \text{ kcal/mole} \sim 10^{-20} \text{ J.}$$

The effective surface area of one polymer unit cell containing two $\text{CH}_2\text{O(POM)}$ units can be estimated to be $4.4\text{\AA} \times 4.05\text{\AA} = 17.8 \text{ \AA}^2$. This gives a value of 5.6×10^{18} for q , the number of polymer units per square meter of particle surface area. In the SD simulation all lengths are nondimensionalized by the particle radius, a . With:

$$\xi = R_0/a \text{ and } \xi_0 = r_e/a,$$

we obtain for Equation (10)

$$F(\xi) = -F_0 \left[\left[\frac{\xi_0}{\xi} \right]^4 - \frac{1}{5} \left[\frac{\xi_0}{\xi} \right]^{10} \right], \quad (13)$$

where F_0 , the amplitude of the L-J force is given by

$$F_0 = \pi^2 q^2 \epsilon a^3 \xi_0^2 = \pi^2 q^2 a \epsilon r_e^2, \quad (14)$$

i.e., the force is particle size dependent and depends linearly on the particle radius. (F_0 has the form of a Hamaker constant [6,7], $A = \pi^2 q^2 \lambda$. The interaction parameter λ contains not only the interaction between a pair of atoms, but also can contain the effect of the medium on the interaction). The total L-J force F_p in Equation (2) is built up by calculating the magnitude of the force for all pairs of particles from Equation (13), computing the vector components dependent on the relative

particle center positions of each pair, and summing all components.

In the SD simulation, Equation (2) is used in dimensionless form [2]. The scaling to dimensionless form introduces the ratio of interparticle forces to the hydrodynamic forces:

$$\frac{F_0}{6\pi\mu a^2\dot{\gamma}} = \frac{\pi^2 q^2 \epsilon a \xi}{6\pi\mu a^2\dot{\gamma}} = \frac{1}{\dot{\gamma}^*} = \frac{\pi q^2 \epsilon r_e^2}{6\mu\dot{\gamma}a} \quad (15)$$

For a particle radius of $a = 0.5 \mu\text{m}$, a suspending fluid viscosity of $\mu = 0.1 \text{ kg/m-s}$, $r_e = 4\text{\AA}$, $\epsilon = 10^{-27} \text{ J}$ and $q = 5.6 \times 10^{18} \text{ C/m}^2$, one obtains

$$\frac{1}{\dot{\gamma}^*} \sim 5 \times 10^5 \frac{1}{\dot{\gamma}} \quad (16)$$

The shear rate $\dot{\gamma} = \Delta U/H$ (in sec^{-1}), where ΔU is the relative tangential velocity of the walls and H is their separation [3], is an input parameter in the SD simulation, controlled by the velocities of the walls and filling factor ϕ ($H = (N\pi/\phi)^{1/2}$, N being the number of particles). $\dot{\gamma}a$ defines the velocity scale in the presence of shear, and $\dot{\gamma}^{-1}$ the time scale [2]. The SD simulations below were performed for $\dot{\gamma}^{-1} = 10^6$.

Equation (15) is a relation between quantities calculated from first principles and macroscopic parameters. It shows that the importance of the L-J interparticle force increases with the square of the polymer coverage per unit area of particle surface. It increases linearly with the L-J attraction well depth ϵ , and the square of the equilibrium

distance r_e . The ratio decreases linearly with the fluid viscosity, the shear rate and the particle radius. An increase in the interparticle force is consistent with an increase in polymer coverage, as it contributes to the total force acting between particle centers from polymer unit interaction (sphere surface) effects. Increasing ϵ , the attractive well depth, also increases the total attractive interparticle force. Increasing r_e , the equilibrium distance, effectively extends the particle separation range over which the L-J attractive forces can act. For larger particles (increase in a), higher viscosities or shear rates, the macroscopic hydrodynamic forces tend to dominate.

Since for very small surface separations, the L-J force changes over a $\sim 10^6$ range, it is clear that the time scale appropriate for hydrodynamic interactions would not capture the L-J force regime, and the ξ^{-4} attraction and ξ^{-10} repulsion in a very small separation range would cause difficult solution convergence problems in the SD simulations. In order to obtain reasonable time steps and acceptable convergence behavior in the L-J interaction region, we linearized the L-J force around the equilibrium separation value of $\xi_e = 0.765\xi_0$. For values of $\xi > 0.0035$, Equation (13) is used, for smaller values

$F(\xi) = -k(\xi - 0.765\xi_0)$ is employed (see Figure 3). The force constant k is determined to yield a smooth transition. A value of $k = 1.7 \times 10^6$ is obtained for computational parameters discussed above. With this procedure the time step used for larger separations required a reduction

by a factor of 10^3 , if very small surface separations are encountered at any time in the SD simulations. It does not seem likely that one can work with much larger time steps if interested in the effect of molecular forces and their interplay with the hydrodynamic force. The decrease in time step size reflects the difference between the micron (particle) and Angstrom region.

III. RESULTS AND DISCUSSION

A. Two - Sphere Simulation Results

To simply illustrate the effect of adding the L-J force to the SD simulations, we first examined a single interacting particle pair. A pair of unit (dimensionless) radius particles are suspended in a liquid subjected to an external gravity force loading and a small shear. The particles are initially separated and arranged as shown in the inset of Figure 4, with the lower particle slightly shifted to the right along the x - axis. Both particles are subjected to normalized sedimentation forces of $F_y = -1.0$ at zero time. An impenetrable wall at $y = 0.0$ constrains the particle centers to $y \geq 0$, forcing a close pair encounter. The linearized L-J interaction parameters for the POM polymer units described previously were used for this simulation. The time integration is allowed to proceed at a fixed large time step (0.025) while the particle center separation is greater than 2.02

(dimensionless) and exceeds the range in which the L-J forces are significant. A 10^{-3} smaller time step was used whenever the distance between particle centers was less than 2.02. Parameters chosen for this simulation are listed in Table 1. Two simulations of two particles each were run, with and without L-J forces to observe qualitative differences in behavior.

From Figure 4 the different behavior in the simulation with (solid line) and without (dashed line) L-J forces is evident. At $t=0.325$ the distance between particle centers becomes less than 2.02. If L-J forces are present, the particle separation very quickly approaches 6.2×10^{-4} ($\sim 3\text{\AA}$). With hydrodynamic forces only, the particle separation decreases smoothly. The time interval Δt over which the pair formation occurs is 1.75×10^{-2} . Since $\gamma=10$ for this simulation, this corresponds to .175 seconds. The energy released in the particle collision calculated from Equation (11) is $\sim 10^{-16}$ J.

B. Simulation of 25 Particles Under Shear

The model suspension consists of a 2-D monolayer of 25 identical spheres in shear flow between two infinite parallel walls of separation H , which are in relative motion to create the uniform shear field. The particles all lie in the x - y plane of the shear field. The use of a 2-D simulation reduces the number of degrees of freedom of the particle with

significant computational savings. Additionally, Brady, et al [3] have shown that the 2-D configuration will qualitatively describe the behavior of 3-D suspensions, and that 25 particles give statistically similar results as 49 particle and larger simulations.

The simulations presented below were performed for particles with a diameter of 1μ , a suspending fluid viscosity of $\mu=0.36$ kg/m-s, a particle filling fraction of $\phi=0.4$ and a shear rate of $\dot{\gamma}=0.14$ sec⁻¹ (see Table 1). Since $\dot{\gamma}$ defines the time scale, the dimensionless units shown in Figures 5 and 6 need to be multiplied by a factor of 7 to obtain the actual time in seconds. Again, two cases were studied: Stokesian Dynamics with hydrodynamic forces only, and Stokesian Dynamics with hydrodynamic and L-J forces. In the cases below, uniform coating of polymer on the spheres was assumed.

The time step for the simple hydrodynamic simulation was 0.025; with L-J forces this was reduced dynamically, depending upon the magnitude of the L-J force, by up to a factor of 10^3 . The smallest time step was therefore 2.5×10^{-5} . Accordingly, a 40 time unit simulation corresponds to about 1.5×10^6 time steps, requiring ~700 hours CPU time on a SUN 3/260 work station.

The pair distribution function would give one measure of structure in suspensions, but it is not necessarily the most important [3]. The

formation of aggregates is far more important in controlling macroscopic properties of suspensions. Figure 5 illustrates the 25 particle suspension microstructure as a function of time. The arrows indicate the direction of the wall motion. The upper row gives snapshots in time of the purely hydrodynamic interactions and its resultant microstructure evolution. The lower row illustrates the evolution of the microstructure with the L-J forces present. Up to time=10, the behavior in both cases is very similar: The formation of particle doublets, triplets, etc., can be observed. From time=20 onward, differences in the microstructure become distinct: In the hydrodynamic case small clusters are observed, but overall the particles are well dispersed. In the L-J case, one large aggregate forms which consists of 23 of the 25 particles which moves to the left as a unit.

The suspension (or effective) viscosity can be defined as the force per unit wall area required to move the wall at a constant velocity divided by the average shear rate. The time evolution of the calculated viscosity based on the average of the top and bottom walls for the two cases described is shown in Figure 6. The viscosity evolution corresponds directly to the evolution of the microstructures described above: up to time=10 the viscosity results are essentially identical. The aggregate formation after time=20 leads to a steep increase in the time - resolved viscosity. The large cluster, encompassing most of the particles, rotates more or less en masse to accommodate itself to the

shear forces and yields a subsequent decrease in viscosity. At later times, the viscosity settles down to a constant value about 1.5 - 2 times larger than for the pure hydrodynamic case. This result suggests that time resolved rheometric experiments with a resolution of about 20 seconds (for this case) would be required for experimental confirmation of the simulation results. This also confirms the results of Brady, et. al., [3] with respect to the correlation between viscosity fluctuations and spanning clusters.

From the results it is clear that the particles, once they fall in the deep attractive well, stick together and don't escape as long as the shear stays the same. Therefore, after this fact is established for a given fluid viscosity, shear rate and particle radius, the long time behavior could be simulated with substantial computer time savings by a rigid joining of the particles at the equilibrium distance r_e . On the other hand, the present method provides a way to investigate the breaking up of particles under increase of shear (deflocculation) and the critical shear rate leading to break up. For future investigations a combination of both approaches seems to be the best solution to study the long-time behavior with a reasonable amount of computer time. It is also clear that other factors such as Brownian motion or surface roughness play a role in the interaction of the particles in a shear flow. In this first study we wanted to keep the number of parameters to a minimum to separate the effect of hydrodynamic and molecular forces.

IV. SUMMARY AND CONCLUSIONS

In this paper we have developed a computational strategy which starts from first principles cluster and band structure calculations and predicts a macroscopic parameter (viscosity) by combining the tools of ab initio quantum mechanics and computational fluid mechanics. In the molecular dynamics - like approach of Stokesian Dynamics developed by Brady et. al., particles in a suspension may interact through both hydrodynamic and non-hydrodynamic forces. We investigated the effect of one non-hydrodynamic force, the L-Jinterparticle force, calculated from first principles for the system of polyoxymethylene and aluminum particles.

It is clear that in this primer a number of simplifying assumption were made:

- the polymer suspension is simulated as a fluid with an effective viscosity,
- the polymeric nature of the suspending fluid is taken into account only in the polymer - polymer and polymer - particle interaction calculations,
- a uniform polymer monolayer coating on the particles is assumed,
- a Lennard - Jones potential is fitted to a potential curve

calculated quantummechanically over a small interaction region,

- the effect of the polymer medium on the L-J interactions is neglected.

Regardless, the QM/SD model is able to correctly predict the macroscopic effects of the subtle, but collective effects of polymer - polymer interactions occurring on the microscopic scale. The QM/SD model can also be systematically improved towards a predictive tool capable of simulating behavior of specific polymer suspensions, and increasing the understanding of the role of suspension and microstructure evolution and particle - polymer interactions which give rise to observed macroscopic parameters and behavior.

ACKNOWLEDGMENT

This work was supported under Office of Naval Research contract N00014-86-C-0724 and Subcontract SK80D7820.

REFERENCES

- [1] M. Seel, A.B. Kunz, and D.T. Wadiak, Phys Rev. B37, 8915 (1988).
- [2] G. Bossis and J.F. Brady, J. Chem. Phys. 80, 5141 (1984); J. Chem. Phys. 87, 5437 (1987).
- [3] J.F. Brady and G. Bossis, Ann. Rev. Fluid Mechanics 20, 111 (1988).
- [4] L. Durlofsky, J.F. Brady and G. Bossis, J. Fluid Mech. 180, 21 (1987).
- [5] L. Durlofsky and J.F. Brady, J. Fluid Mech. 200, 39 (1989).
- [6] E.J.W. Verwey and J.Th.G. Overbeck, Theory of the Stability of Lyophobic Colloids, Elsevier, Amsterdam, (1948).
- [7] R.D. Vold and M.J. Vold, Colloid and Interface Chemistry (Addison - Wesley, Reading (1983)).
- [8] B. Derjaguin, Kolloid - Z, 69, 155 (1934).
- [9] H.C. Hamaker, Physica 4, 1058 (1937).

Table 1: SD simulation parameters for the two particle and 25 particle simulations with L-J forces

Number of Particles	2	25
Particle Diameter (μ)	1	1
Filling Factor ϕ	0.02	0.40
Suspending Fluid Viscosity μ (kg/m-s)	0.5	0.36
Applied Shear Rate $\dot{\gamma}$ (sec ⁻¹)	0.10	0.14
$1/\dot{\gamma}^*$ in Equation (15)	10^6	10^6

Figure Captions

- Figure 1. Geometry for the calculation of the Lennard - Jones forces between one polymer unit and an infinitely large plane.
- Figure 2. Geometry used in the Derjaguin procedure for the calculation of the Lennard - Jones forces between two spheres.
- Figure 3. The L-J force and its linearization for very small surface separations.
- Figure 4. Interparticle distance versus time for the two particle simulation with (solid line) and without (dashed line) an interparticle Lennard - Jones potential.
- Figure 5. Snapshots of instantaneous particle configurations for the sheared suspension of 25 particles. Top row: hydrodynamics forces only. Bottom row: additional Lennard - Jones forces.
- Figure 6. Time evolution of the suspension (effective) viscosity for the sheared suspension of Figure 8. ----- indicates the viscosity for the hydrodynamic forces only, -.-.-. indicates the viscosity if Lennard - Jones forces are present.

